International Journal of
Molecular Sciences

MDPI

Article

Exploring the Role of Platelets in Virus-Induced Inflammatory Demyelinating Disease and Myocarditis

Ijaz Ahmad [1,†], Seiichi Omura [1,†], Fumitaka Sato [1], Ah-Mee Park [1,2], Sundar Khadka [1,3], Felicity N. E. Gavins [4], Hiroki Tanaka [5], Motoko Y. Kimura [6] and Ikuo Tsunoda [1,*]

1 Department of Microbiology, Faculty of Medicine, Kindai University, 377-2 Ohnohigashi, Osakasayama, Osaka 589-8511, Japan; ijazahmad383@gmail.com (I.A.); somura@med.kindai.ac.jp (S.O.); fsato@med.kindai.ac.jp (F.S.); ampk@med.kindai.ac.jp (A.-M.P.); cls.sundar@gmail.com (S.K.)
2 Department of Arts and Sciences, Faculty of Medicine, Kindai University, Osaka 589-8511, Japan
3 Department of Immunology, Duke University, Durham, NC 27708, USA
4 Department of Biosciences, Centre for Inflammation Research and Translational Medicine, College of Health and Life Sciences, Brunel University London, Uxbridge UB8 3PH, UK; felicity.gavins@brunel.ac.uk
5 Division of Tumor Pathology, Department of Pathology, Asahikawa Medical University, Asahikawa 078-8510, Japan; hiroki-t@asahikawa-med.ac.jp
6 Department of Experimental Immunology, Graduate School of Medicine, Chiba University, Chiba 263-8522, Japan; kimuramo@chiba-u.jp
* Correspondence: itsunoda@med.kindai.ac.jp
† These authors contributed equally to this work.

Abstract: Theiler's murine encephalomyelitis virus (TMEV) infection has been used as a mouse model for two virus-induced organ-specific immune-mediated diseases. TMEV-induced demyelinating disease (TMEV-IDD) in the central nervous system (CNS) is a chronic inflammatory disease with viral persistence and an animal model of multiple sclerosis (MS) in humans. TMEV infection can also cause acute myocarditis with viral replication and immune cell infiltration in the heart, leading to cardiac fibrosis. Since platelets have been reported to modulate immune responses, we aimed to determine the role of platelets in TMEV infection. In transcriptome analyses of platelets, distinct sets of immune-related genes, including major histocompatibility complex (MHC) class I, were up- or downregulated in TMEV-infected mice at different time points. We depleted platelets from TMEV-infected mice by injecting them with platelet-specific antibodies. The platelet-depleted mice had significantly fewer viral antigen-positive cells in the CNS. Platelet depletion reduced the severities of TMEV-IDD and myocarditis, although the pathology scores did not reach statistical significance. Immunologically, the platelet-depleted mice had an increase in interferon (IFN)-γ production with a higher anti-TMEV IgG2a/IgG1 ratio. Thus, platelets may play roles in TMEV infection, such as gene expression, viral clearance, and anti-viral antibody isotype responses.

Keywords: glycoprotein Ib α chain; bioinformatics analysis; RNA sequencing analyses; regulation of gene expression; dilated cardiomyopathy; neuroinflammatory disease; picornavirus infections

Citation: Ahmad, I.; Omura, S.; Sato, F.; Park, A.-M.; Khadka, S.; Gavins, F.N.E.; Tanaka, H.; Kimura, M.Y.; Tsunoda, I. Exploring the Role of Platelets in Virus-Induced Inflammatory Demyelinating Disease and Myocarditis. *Int. J. Mol. Sci.* **2024**, *25*, 3460. https://doi.org/10.3390/ijms25063460

Academic Editor: Antonietta Bernardo

Received: 20 February 2024
Revised: 14 March 2024
Accepted: 16 March 2024
Published: 19 March 2024

1. Introduction

Viral infection can cause tissue damage directly by infected cell lysis (viral pathology) or indirectly by the host's immune responses to the pathogen (immunopathology) [1]. Several virus-induced diseases have also been shown to result from both viral pathology and immunopathology to some extent. The tissue tropism of viruses has often determined the target organs in viral infections; most viruses have been shown to have an affinity for specific tissues and only infect their target organ. For example, poliovirus can selectively infect and damage motor neurons that express poliovirus receptors in the central nervous system (CNS). Coxsackievirus B (CVB) can infect the heart and induce viral myocarditis [2]. Severe acute respiratory syndrome coronavirus 2 (SARS-CoV-2) has been shown to infect

not only the respiratory system but also the CNS and other general organs, including the heart, inducing CNS pathology and myocarditis [3].

Viral tropism and the pathogenesis of distinct organs have been studied using animal models with various viruses with different tropisms. Theiler's murine encephalomyelitis virus (TMEV) is a non-enveloped, positive-sense, single-stranded RNA virus that belongs to the family *Picornaviridae* and genus *Cardiovirus*, and is a natural pathogen of mice [4–6]. Following the viral inoculation, TMEV can infect both the CNS andheart, causing CNS and cardiac inflammation [7] (Figure 1). Thus, TMEV infection is a unique experimental system to clarify organ-specific viral-induced inflammatory diseases.

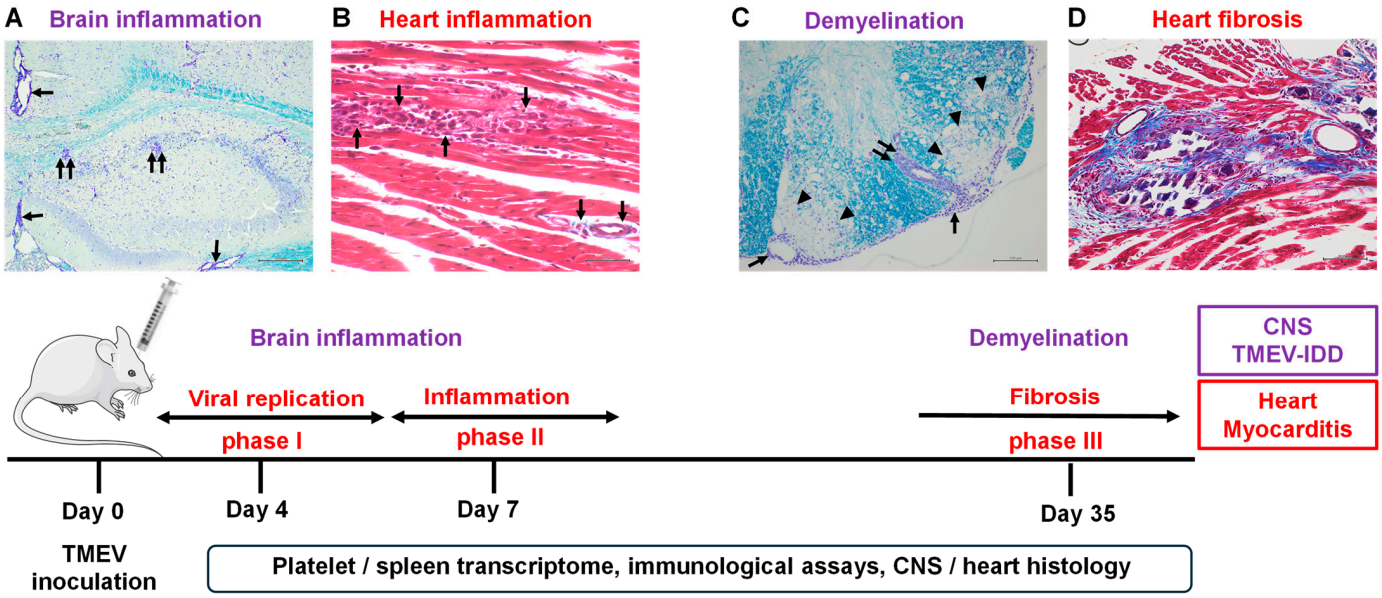

Figure 1. Schematic representation of the time course and experiments of Theiler's murine encephalomyelitis virus (TMEV) infection. (**A**,**C**) In the central nervous system (CNS), following virus inoculation, TMEV initially infects neurons in the gray matter of the brain and causes inflammation (polioencephalitis). Later, around 1 month post infection (p.i.), TMEV persistently infects the white matter of the spinal cord and induces inflammatory demyelination. In Luxol fast blue stain, the arrowheads, arrows, and paired arrows indicate demyelination, meningitis, and perivascular cuffing (inflammation), respectively. Scale bars: (**A**) 200 μm; and (**C**) 100 μm. (**B**,**D**) TMEV-induced myocarditis can be divided into three phases. In phase I (around 4 days p.i.), TMEV directly attacks cardiomyocytes by infecting and replicating (viral pathology). In phase II (around 1 week p.i.), anti-viral T cell and antibody responses are induced, which not only clear the virus but also damage cardiomyocytes (immunopathology). In phase III (around 1 month p.i.), when the tissue damage caused in phases I and II is severe, it leads to cardiac fibrosis. In Masson's trichrome stain, the arrows indicate cardiac inflammation; the blue and dark purple colors show fibrosis and calcification, respectively. Scale bars: (**B**) 50 μm; and (**D**) 100 μm. (Bottom) Experimental designs of this study. We intracerebrally inoculated mice with TMEV and harvested the spleen and platelet samples for transcriptome analyses, sera and lymphocytes for immunological assays, and the CNS and heart tissues for histological analyses 4, 7, and 35 days p.i.

Experimentally, TMEV infection has been used as a viral model of multiple sclerosis (MS), since TMEV can induce a chronic inflammatory demyelinating disease [TMEV-induced demyelinating disease (TMEV-IDD)] in the CNS of susceptible mouse strains, such as SJL/J and C3H mice [8]. Following intracerebral TMEV inoculation, TMEV initially infects the gray matter of the brain, inducing inflammation (Figure 1A). Later, around 1 month post infection (p.i.), TMEV persistently infects macrophages and glial cells, including oligodendrocytes and microglia [9], with the infiltration of lymphocytes and macrophages, inducing inflammatory demyelination in the white matter of the spinal cord

(Figure 1C) [4,9]. Although anti-viral antibodies and $CD4^+$ and $CD8^+$ T cells have been shown to be essential in viral clearance, these immune effectors can also play pathogenic roles in demyelination [10]. Thus, TMEV-IDD is similar to MS immunologically and histologically. Although the precise pathomechanism of MS is still unknown, the viral etiology of MS has been supported clinically and epidemiologically. For example, several viruses, including human herpesvirus 6 (HHV-6), Epstein–Barr virus (EBV), and picornaviruses, have been detected in MS samples [11]. EBV has been identified as a potential environmental trigger of MS; immune responses to EBV were higher in MS patients than in a healthy population [12,13].

TMEV infection has also been used as a mouse model of viral myocarditis [14]. Myocarditis is an inflammatory disease of the heart [15,16] and can be caused by a variety of viruses, such as human immunodeficiency virus (HIV) and hepatitis C virus (HCV), in humans [17–19]. Picornaviruses, particularly CVB, are a well-known pathogen of myocarditis [20]. Viral myocarditis can be divided into three distinct phases. TMEV-induced myocarditis has been shown to develop all three phases: in phase I, acute viral infection (around 4 days p.i.), the virus directly infects and replicates in the cardiac muscles and damages cardiomyocytes (viral pathology). Activated innate immune responses against the virus are involved in the viral clearance and recruitment of immune cells. In phase II, anti-viral cellular and humoral responses are activated (around 1 week p.i.); anti-viral immune responses not only eradicate the virus but also damage cardiomyocytes (immunopathology). In phase III (around 1 month p.i.), when the cardiac tissue damage is severe in phases I and II, it results in cardiac fibrosis and remodeling without viral persistence in the heart [21]. Although the precise pathomechanism of human and experimental myocarditis is unclear, an immunomodulating therapy without suppressing anti-viral immune responses has been suggested for the treatment of viral myocarditis [22–24].

Previously, we conducted a transcriptome analysis using blood and heart samples from TMEV-infected mice to identify the phase-specific gene expressions during the disease course of myocarditis [14,24]. Unexpectedly, we found the upregulation of seven platelet-related genes, including pro-platelet basic protein (*Ppbp*), platelet factor 4 (*Pf4*), and platelet glycoprotein IX (*Gp9*), in blood of TMEV-infected mice in phase III [24,25] (Supplemental Table S1). On the other hand, in an autoimmune model of MS, experimental autoimmune encephalomyelitis (EAE), Mehmood et al. (2023) conducted data mining using the spleen transcriptome data from two EAE models with distinct pathomechanisms induced in SJL/J and A.SW mice [26]. They reported the enriched gene ontology "platelet alpha-granule" and the enriched pathway "platelet activation" in EAE mice sensitized with the myelin oligodendrocyte glycoprotein $(MOG)_{92–106}$ peptide; the upregulated genes included platelet-derived growth factor alpha (*Pdgfra*), megakaryocyte and platelet inhibitory receptor G6b (*Mpig6b*) [27], *Pf4* [28], and phospholipase A2 group VII (*Pla2g7*) [26]. The transcriptome data used by Mehmood et al. were our own experimental data deposited in the Gene Expression Omnibus (GEO) previously (Accession number: GSE99300) [29]. Thus, we reanalyzed the data and confirmed that platelet-related genes were upregulated in the spleen of two EAE models: 11 genes in SJL/J mice and five genes in A.SW mice. Intriguingly, although two EAE models had a primary progressive disease course clinically, only *Pdgfra* and *Pla2g7* were commonly upregulated in the two models (Supplemental Table S1). When we compared the seven upregulated genes in TMEV infection, the SJL/J EAE model had three genes, 1) multimerin 1 (*Mmrn1*) [30], 2) *Mpig6b*, and 3) *Pf4*, commonly upregulated, although the A.SW EAE model had no similarity with the seven upregulated genes in TMEV infection (Supplemental Table S1). Since platelets have been detected in lesions in EAE and MS previously [31], in this study, we focused on the role of platelets in TMEV infection.

Although platelets are known for their main roles in hemostasis and thrombosis, platelets can contribute to virus-induced inflammatory diseases by (1) binding virions and (2) modulating immune responses. First, platelets have been shown to express various viral receptors, facilitating direct interactions with viruses, such as influenza virus, CVB, and

SARS-CoV-2 [32–34]. Several viruses have been reported to indirectly interact with platelets by the formation of virus and immunoglobulin (Ig) complexes, which are recognized by Fcγ receptor IIA on platelets [32]. Although platelet binding to viruses can lead to viral clearance [35], several viruses, including HCV and CVB, have been shown to use platelets as a vehicle for viral dissemination or replication within platelets [36–39].

Second, platelets have been shown to play various immunological roles in inflammatory diseases. For example, activated platelets can reach the sites of infection where they can modulate immune processes via expressions of immune molecules on their membrane, such as major histocompatibility complex (MHC) class I and CD40 ligand [40]. Platelets have been shown to contain various mRNAs, translate several proteins, and transport various inflammatory proteins or mRNAs, including chemokines and cytokines, to inflammatory sites [41–44]. Anti-platelet treatment, such as the administration of platelet-depletion antibodies, has been shown to modulate virus-induced inflammation experimentally [45,46].

In this study, we aimed to determine the role of platelets in the pathogenesis of TMEV-IDD and TMEV-induced myocarditis. Using RNA sequencing (RNA-seq), we found that distinct sets of immune-related genes, including MHC class I, were up- or downregulated in platelets at different time points; TMEV genomes were not detectable in the platelets at any time point. Platelet depletion in vivo in TMEV infection reduced viral persistence in the CNS and ameliorated histological severities by reducing inflammatory lesions in the spinal cord and fibrotic areas in the heart of TMEV-infected mice. Platelet depletion also increased interferon (IFN)-γ production and altered anti-viral IgG isotype responses, which could play a role in reduced viral persistence. Thus, platelets could be a new therapeutic target for MS and viral myocarditis.

2. Results

2.1. Expressions of Immune Genes Are Altered in the Spleen of TMEV-Infected Mice

During the first week of TMEV infection, viremia and TMEV-specific immune responses are observed. Then, innate and acquired immune responses eradicate the virus from the subject's general organs by 2 weeks p.i., although the virus can persistently infect the spinal cord. We isolated mRNA from the spleen and platelets from TMEV-infected and control mice 4, 7, and 35 days p.i. By computational analyses of RNA-seq data, we compared the transcriptomes among the samples.

First, we conducted a two-way comparison analysis of splenic gene expressions between TMEV-infected and control mice at each time point (Figure 2A–C). In the spleen, heat maps showed the upregulations of innate immune genes, including 2′,5′-oligoadenylate synthetase (*Oas*) and interferon-induced protein with tetratricopeptide repeats (*Ifit*), 4 and 7 days p.i. as well as acquired immune genes, particularly Igs, 7 days p.i. Several other acquired immune genes, such as Igs and T cell receptors (TCRs), were upregulated 35 days p.i.; the transcriptome data of several immune molecules, including granzyme B, C-X-C motif chemokine ligand 10 (*Cxcl10*), the IgA heavy chain (*Igha*), and the IgG2c heavy chain (*Ighg2c*), were validated by real-time PCR testing (Supplemental Figure S1). Using the Database for Annotation, Visualization, and Integrated Discovery (DAVID), we identified the functional clusters of differentially expressed genes (DEGs) in TMEV infection (Supplemental Table S2). A total of 80 and 135 genes were up- and downregulated 4 days p.i., respectively; 230 and 41 genes were up- and downregulated 7 days p.i., respectively; and 18 and 267 genes were up- and downregulated 35 days p.i., respectively. As expected, the DAVID functional clustering of DEGs showed that the immune system process-related pathways were activated 4 and 7 days p.i.

To further clarify the time course patterns of gene clusters, we conducted *k*-means clustering and divided the genes into 15 clusters based on the gene expression patterns (Supplemental Tables S3 and S4; Figure 2D); an appropriate number of clusters was determined based on the Davies–Bouldin indexes (Supplemental Table S3). We examined the function of genes in each cluster with the DAVID (Supplemental Table S4). In a radar chart of the fifteen clusters, four clusters (clusters 1, 7, 10, and 12) changed the expressions

at only one time point. Eleven clusters included genes whose expressions were changed at two or three time points. For example, cluster 6, composed of innate immune genes, including IFN-induced genes, was upregulated 4 and 7 days p.i.; cluster 14, consisting of various Ig and TCR genes, was upregulated 7 days p.i.; and cluster 15, composed of a smaller number of distinct Ig and TCR genes, was upregulated 35 days p.i. (Supplemental Table S3, Figure 2D,E).

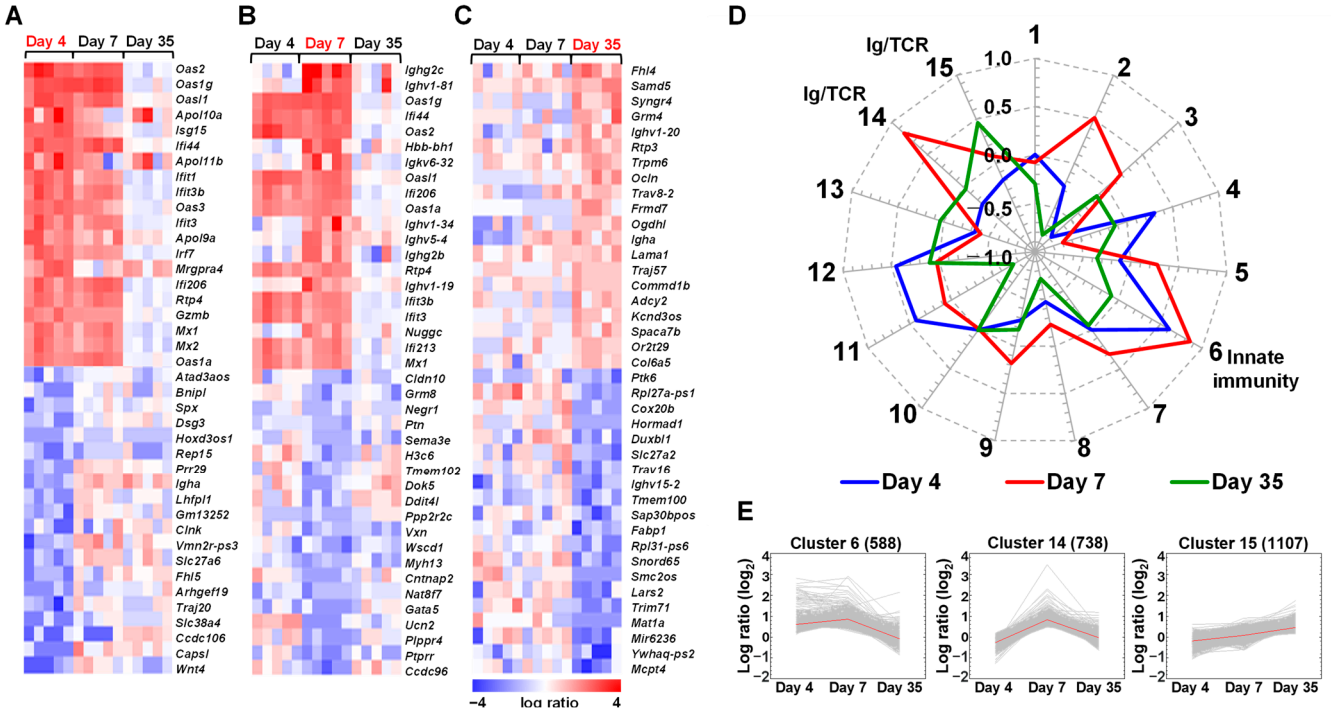

Figure 2. Transcriptome analyses of the spleen from TMEV-infected mice. (**A**–**C**) We created heat maps of the top 20 up- and downregulated genes 4 (**A**), 7 (**B**), and 35 (**C**) days p.i. The red, blue, and white colors indicate upregulation, downregulation, and no change, respectively, compared with the control samples. Each column represents the data from one mouse (five mice/time point). (**D**) We conducted *k*-means clustering and divided the genes into the 15 clusters based on their expression patterns. In a radar chart of the 15 cluster centers, radial axis values are fold-changes in the cluster center gene expressions compared with controls, which ranged from −1 to 1. These values are shown in binary logarithm ($\log_2$): −1, two-fold downregulation; 0, no change; and 1, two-fold upregulation, compared with controls. Cluster 6, composed of innate immune genes, including interferon (IFN)-induced genes, was upregulated 4 and 7 days p.i. Cluster 14, consisting of various immunoglobulin (Ig) and T cell receptor (TCR) genes, was upregulated 7 days p.i.; and cluster 15, composed of a smaller number of distinct Ig and TCR genes, was upregulated 35 days p.i. (**E**) Expression patterns of clusters 6, 14, and 15 showed the temporal gene expressions at each time point; the red lines indicate the cluster centers. The number of genes in each cluster is shown at the top of each cluster.

2.2. Distinct Gene Expressions, Including Immune-Related Genes, in Platelets of TMEV-Infected Mice

Using the platelet samples from the TMEV-infected and control mice, we also conducted transcriptome analyses at the three time points of TMEV infection. Although we examined whether TMEV genomes were detected from the platelet transcriptome data of the TMEV-infected mice (Supplemental Figure S2), no viral genomes were detected in the platelets at any time point. Our heat maps showed up- and downregulations of distinct genes at each time point (Figure 3A–C), including changes in immune-related genes (e.g., the upregulation of *H-2D1* 4 and 7 days p.i. and the downregulation of *Cd55* and *Cd52* 35 days p.i.). A total of 51 and 35 genes were up- and downregulated 4 days p.i., respectively; 92 and 39 genes were up- and downregulated 7 days p.i., respectively; and

130 and 209 genes were up- and downregulated 35 days p.i., respectively. Although we attempted to identify the genes in the functional pathways using the DAVID, the enrichment scores of identified pathways were lower than those in the spleen samples; immune-related pathways were not ranked among the top five pathways (Supplemental Table S5).

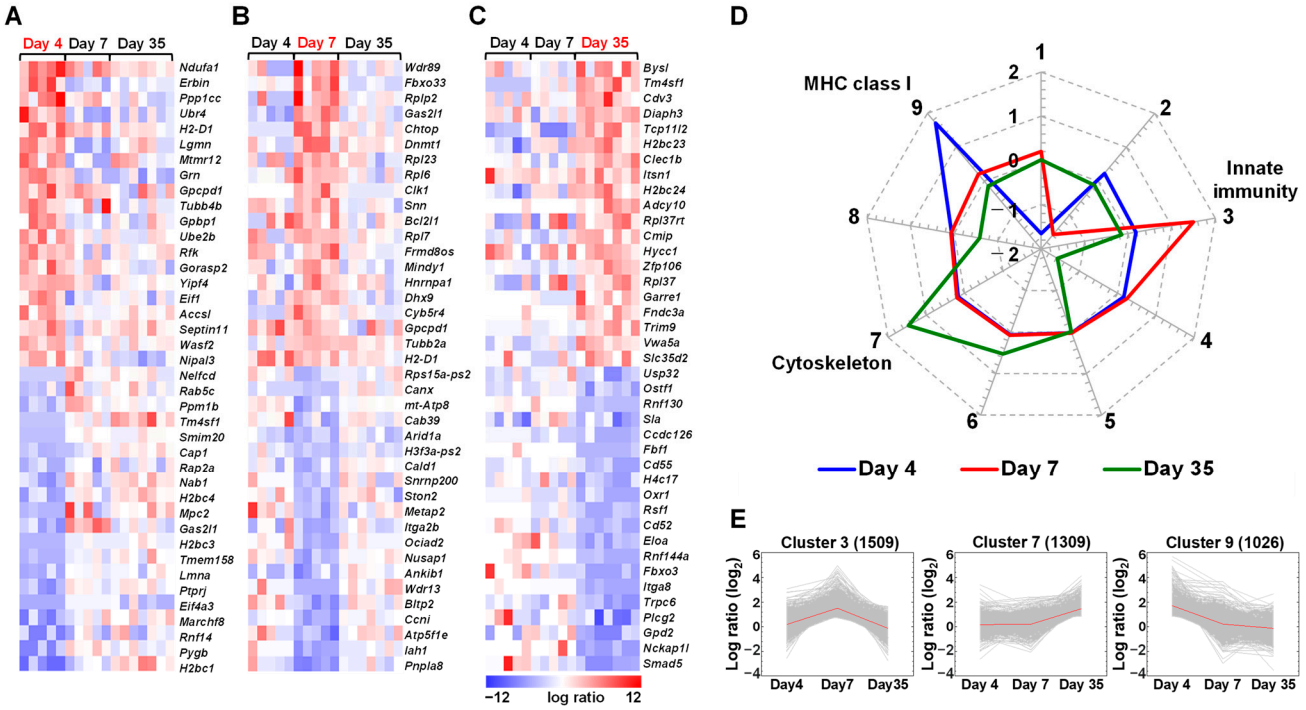

Figure 3. Transcriptome analyses of the platelets from TMEV-infected mice. (**A**–**C**) We created heat maps of the top 20 up- and downregulated genes 4 (**A**), 7 (**B**), and 35 (**C**) days p.i. The red, blue, and white colors indicate upregulation, downregulation, and no change, respectively, compared with the control samples. (**D**) We conducted *k*-means clustering and divided the genes into nine clusters based on their expression patterns. A radar chart using the nine cluster centers showed the distinct expression patterns of the platelet transcriptomes at each time point. Radial axis values are the cluster center gene changes compared with controls, which ranged from −2 to 2 and are shown in $\log_2$: −2, four-fold downregulation; 0, no change; and 2, four-fold upregulation, compared with controls. Genes in four clusters (clusters 4, 6, 7, and 8) changed their expressions at one time point. Genes in cluster 5 had few changes. Four clusters (clusters 1, 2, 3, and 9) included genes changed at two or three time points. (**E**) Expression patterns of three clusters (clusters 3, 7, and 9) showed the temporal gene expression patterns at each time point; the red lines indicate the cluster centers. Number of genes in each cluster is shown at the top of each cluster. Each time point was composed of five to seven mice.

Using *k*-means clustering and the DAVID, we classified the genes into nine clusters (Supplemental Tables S6 and S7; Figure 3D). MHC class I (*H-2D1*, *H-2K1*, and several *H-2Q* genes) [47] and β_2 microglobulin (*B2m*) genes were upregulated in cluster 9 4 days p.i. Some innate immune genes, such as IFN-activated genes, were upregulated in cluster 3 7 days p.i. Microtubule-related genes, such as tubulin beta 2B class IIB (*Tubb2b*) and dynein axonemal heavy chains (*Dnah*), which are associated with the morphology and function of platelets [48], were highly upregulated in cluster 7 35 days p.i. Immune-related genes, including *Cd55*, *Itga8* [49], *Cd52*, and *Il16* [50], were downregulated in cluster 4.

2.3. Overall Gene Expression Profiles Differ in the Spleens, but Not in the Platelets between TMEV-Infected and Control Mice

Using a principal component analysis (PCA) of transcriptome data, we investigated whether the overall gene expression profiles differed between the TMEV-infected and

control mice at each time point. In the spleen, the samples were separated significantly by principal component (PC) 2 values between the TMEV-infected and control groups 7 and 35 days p.i., but not 4 days p.i. (Figure 4A). A PCA using the splenic transcriptomes of the TMEV-infected mice separated the samples at each time point into three distinct groups (Supplemental Figure S3A). The PC1 values 35 days p.i. were significantly higher than those 4 and 7 days p.i. (*, $p < 0.05$, ANOVA, Supplemental Figure S3B); the PC2 values 7 days p.i. were significantly lower than those 4 and 35 days p.i. (***, $p < 0.001$, ANOVA, Supplemental Figure S3C). Factor loading for PC1 and PC2 showed that genes contributing to the PC1 and PC2 values included various immune-related molecules, such as Ig genes, reflecting changes in anti-viral immune responses at each time point (Supplemental Figure S3D,E). On the other hand, the PCA of the splenic transcriptome data of the control mice did not separate the groups of samples at each time point (Supplemental Figure S4).

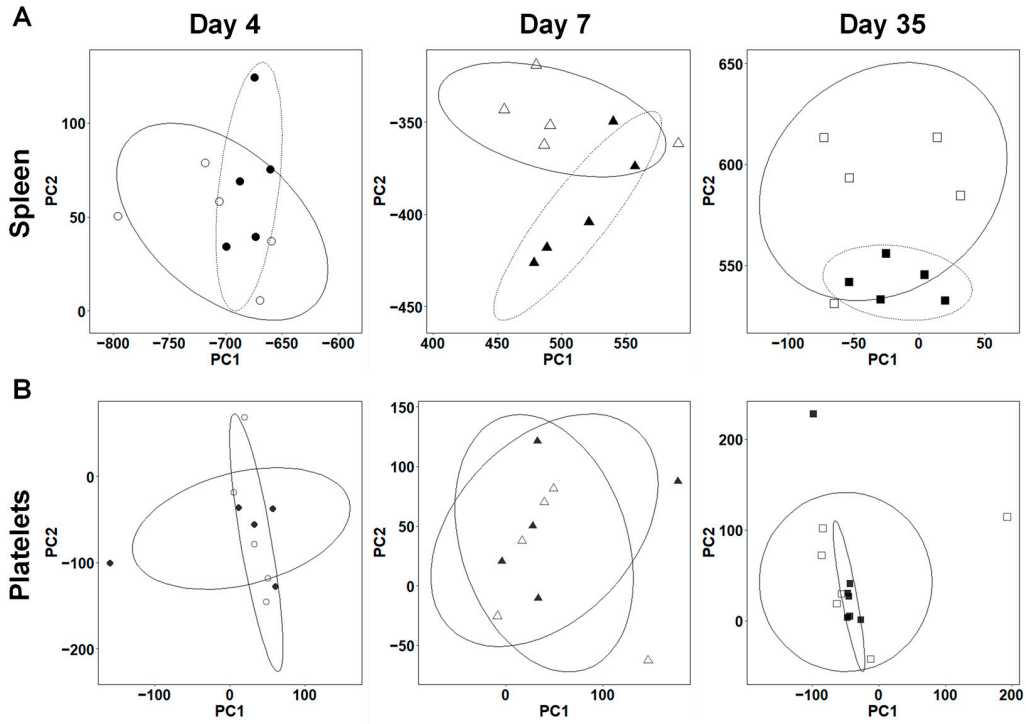

Figure 4. Principal component analysis (PCA) of splenic and platelet transcriptome data between TMEV-infected and control mice at each time point. (**A**) In the spleen, the samples were separated significantly by principal component (PC) 2 values between the TMEV-infected and control groups 7 days p.i.: TMEV (▲), −394.33 ± 14.32; control (△), −347.48 ± 7.95, $p < 0.05$, and 35 days p.i.: TMEV (■), 541.66 ± 4.30; control (□), 587.18 ± 15.10, $p < 0.05$, but not 4 days p.i.: TMEV (●), 68.42 ± 16.09; control (○), 46.06 ± 12.16, $p = 0.348$. (**B**) In platelets, the samples were not separated into distinct groups at any time point.

In the platelets, the PCA of the transcriptome data did not separate the samples between the TMEV-infected and control groups at any time point (Figure 4B). Thus, the individual gene expression changes (Figure 3) in TMEV infection were not significant enough to alter the overall transcriptome profiles (Figure 4B) of the platelets at any time point. On the other hand, when we conducted a PCA using the transcriptome data from the three time points, the PCA separated the samples into two groups: one group was composed of the samples 4 and 7 days p.i., and the other was composed of the samples 35 days p.i. (Figure 5A,B). We also conducted a PCA using all the TMEV-infected and control platelet transcriptome data; we did not see separations between the TMEV-infected and control samples (Supplemental Figure S5). We found that the overall gene expression patterns of the samples from days 4 and 7 versus those of day 35 differed, which likely reflected the maturation-related gene expression changes in the platelets.

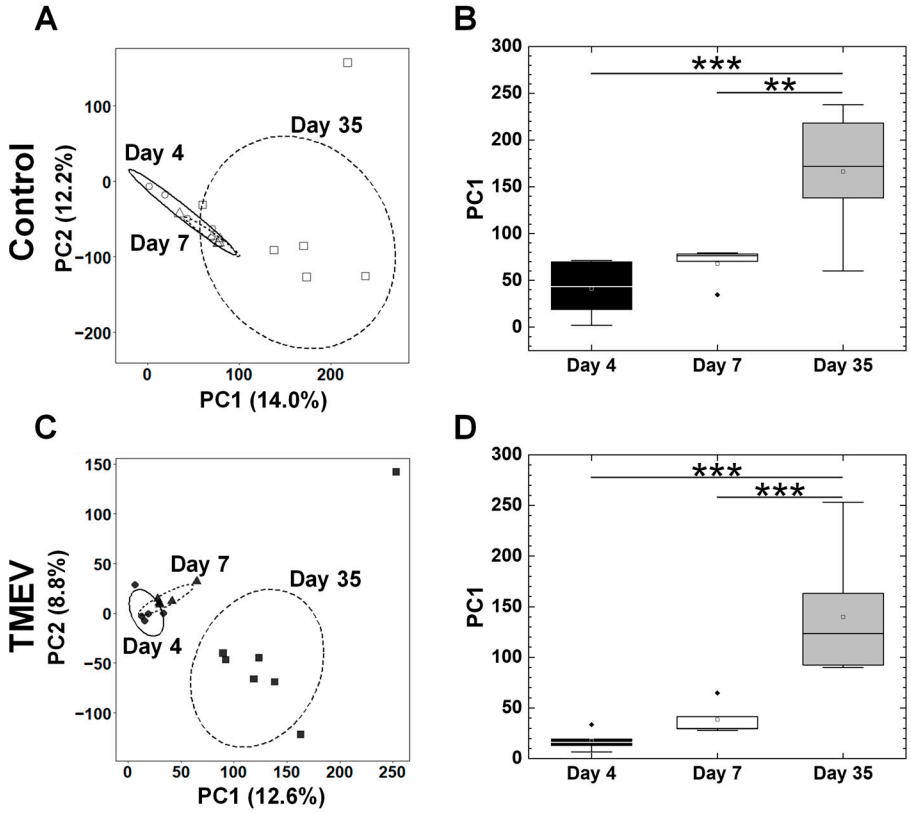

Figure 5. PCA of the platelet transcriptome data from TMEV-infected and control mice on day 4 (TMEV, ●; control, ○), day 7 (TMEV, ▲; control, △), and day 35 (TMEV, ■; control, □). (**A**,**B**) In the control samples, a PCA separated the samples into two groups: one group was composed of days 4 and 7 samples, and the other was composed of day 35 samples. The values in parenthesis indicated the proportion of variance of each PC. When the PC1 values were compared among the three time points, the PC1 values of day 35 samples were significantly different from those of days 4 and 7 samples (**, $p < 0.01$; ***, $p < 0.001$, ANOVA). (**C**,**D**) In the TMEV-infected samples, PCA and their PC1 values at each time point showed similar profiles to the control samples. In the boxplots: the open square, middle line, box, lower whisker, upper whisker, and closed rhombus indicate the mean, median, interquartile range, minimum, maximum, and outlier, respectively. The total sample number was five to seven per time point.

2.4. Platelets Are Present in the CNS and Heart of TMEV-Infected Mice

To determine whether platelets could play a role in the CNS and cardiac pathologies in TMEV infection, we killed the TMEV-infected mice 4, 7, 21, and 35 days p.i. and visualized the platelets using immunohistochemistry against platelet-specific markers, CD42b [platelet glycoprotein Ib α chain (GPIbα)] and CD61 (integrin β3) [51] (Figure 6). We also immunostained uninfected normal tissue sections as well as inflammatory CNS demyelinating lesions of mice with EAE, an autoimmune model of MS, in which platelet accumulations in the CNS have been reported previously [31]. In uninfected mice, we detected few or no platelets in the CNS and a small number of platelets in the heart (Figure 6A,C), since we perfused the mice extensively, removing their blood when we made histology sections. As a positive control, we used platelet-producing megakaryocytes (Supplemental Figure S6A). In EAE induced with the myelin proteolipid protein $(PLP)_{139–151}$ or $MOG_{35–55}$ peptide, we found a small number of platelets in the luminal side of the vascular endothelia, but not in the parenchyma adjacent to CNS inflammatory lesions (Supplemental Figure S6B,C).

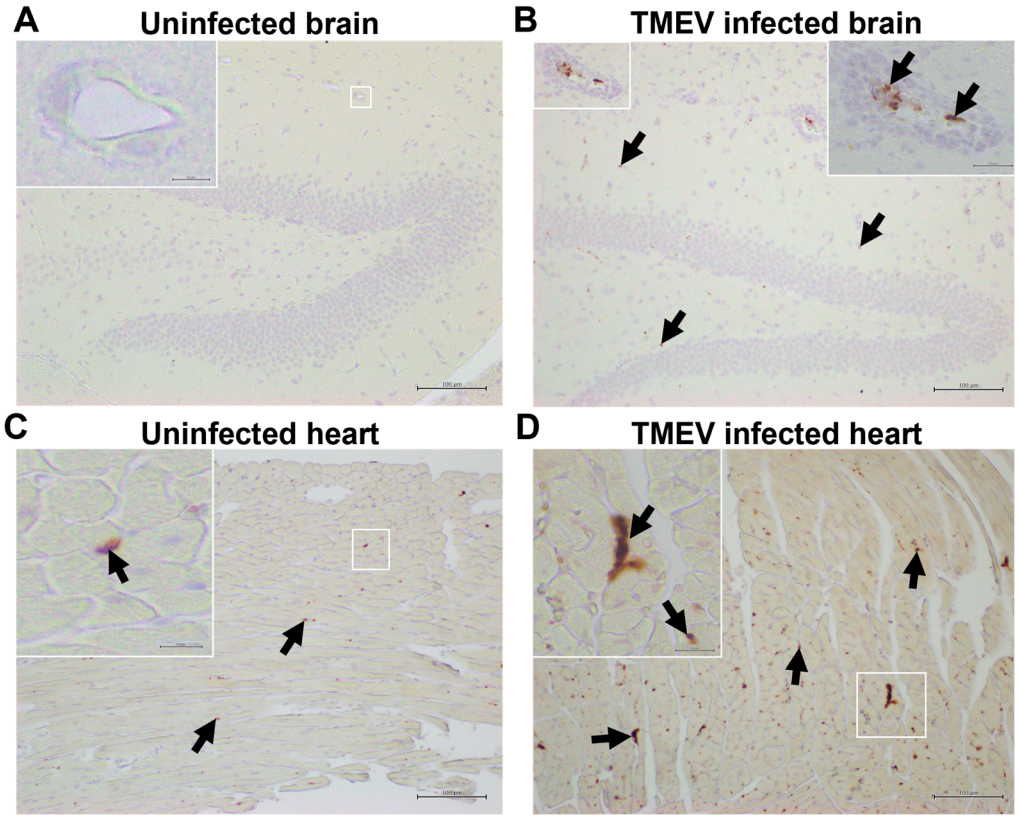

Figure 6. Platelet detection in the brain and heart of TMEV-infected mice. (**A**,**C**) We killed the uninfected mice and conducted immunohistochemistry against the platelet glycoprotein Ibα (GPIbα/CD42b) using brain and heart sections. We could not detect platelets in the brain of uninfected mice, although we detected a small number of platelets (arrows) in the heart. (**B**,**D**) We killed TMEV-infected mice 7 days p.i. and detected platelets attached to the luminal side of vascular endothelia in the brain and more diffusely in the heart. (**A**,**B**) hippocampus; and (**C**,**D**) heart**.** Scale bar: (**A**–**D**) 100 µm; and inset, 50 µm.

In the CNS of TMEV-infected mice, we detected a small number of platelets sporadically, attached to the luminal side of the vascular endothelia in the inflammatory brain lesions 4 and 7 days p.i. (Supplemental Figure S6D,E, Figure 6B), and a much smaller number of platelets attached to the vessels in the spinal cord 21 and 35 days p.i. (Supplemental Figure S6F). In the heart of the TMEV-infected mice, we detected more substantial platelet accumulations than in their CNS; the platelets were observed diffusely, independent of cardiac lesions. The platelet accumulations in the heart peaked 7 days p.i. (Figure 6D), although a lower number of platelets was detected 4 days and 3 weeks p.i. (Supplemental Figure S6G–I) [14]. Thus, in the CNS and heart of the TMEV-infected mice, we found platelets adjacent to inflammatory lesions, although we did not see a parenchymal infiltration of platelets in either their CNS or heart.

2.5. Platelets' Depletion Reduces Viral Persistence in TMEV-IDD

Using an antibody against GPIbα, we determined whether platelet depletion could alter TMEV-IDD histologically. We depleted the platelets by injecting the mice with an anti-GPIbα antibody; we found that a single injection of the anti-GPIbα antibody depleted 98.6% of the platelets in four days (Supplemental Figure S7A). To investigate the role of platelets in TMEV-infected mice, we injected the anti-GPIbα-antibody intravenously (i.v.) 0 and 5 days p.i. (early group) or 18 and 22 days p.i. (late group). The control group received the control IgG antibody. We killed the TMEV-infected mice 35 days p.i. and compared the number and distribution of viral antigen-positive (antigen^{+}) cells by immunohistochemistry

with an anti-TMEV antibody among the three groups. In all groups, the viral antigen$^+$ cells were mainly detected in the white matter of the ventral and lateral funiculi of the spinal cord with minimal involvement of the dorsal funiculus, as reported previously in TMEV-IDD [52] (Figure 7A). We detected a significantly smaller total number of viral antigen$^+$ cells in the early and late groups than in the control group (Figure 7B, overall, *, $p < 0.05$ and **, $p < 0.01$, ANOVA). In the ventral funiculus, viral antigen+ cells were significantly smaller in the early group (*, $p < 0.05$, ANOVA); in the lateral funiculi, there were significantly fewer in the early and late groups than in the control group (*, $p < 0.05$, ANOVA). On the other hand, there were few viral antigen+ cells in the dorsal funiculus, and there were no statistical differences among all the groups (Figure 7B). Thus, although platelet depletion reduced the number of viral antigen$^+$ cells, it did not change the spatial distribution of the viral antigen$^+$ cells in the spinal cord. We also quantified the spinal cord pathology scores 35 days p.i. The levels of demyelination and overall pathology were lower in the early group than in the control group ($p = 0.098$, $p = 0.088$, ANOVA); there were no statistically differences between the late and control groups (Figure 7C). There were also no statistical differences in meningitis among all groups, although the late group had higher scores of perivascular cuffing compared with the early and control groups (*, $p < 0.05$, $p = 0.053$, ANOVA).

2.6. Platelets Contribute to the Pathogenesis of Myocarditis

The TMEV-infected mice had multiple focal fibrotic lesions with calcification in their hearts 35 days p.i.; only a small number of infiltrating immune cells were sporadically detectable (Figure 8A) as reported previously [14]. We used picrosirius red staining for visualizing collagens I and III (Figure 8B). We also examined the T cell infiltration in the heart with immunohistochemistry against CD3 (Figure 8C). Our quantification of the fibrotic areas showed that the early and late groups had smaller lesion areas than the control group (Figure 8D). Although only a small number of T cells were sporadically detectable in all groups; we detected more CD3$^+$ T cells in the early group (**, $p < 0.01$, ANOVA) than in the control and late groups (Figure 8E).

2.7. Platelet Depletion Alters Antibody Isotype Responses

We collected the sera from the TMEV-infected mice 35 days p.i. and compared antiviral IgG isotype titers among the three groups, using enzyme-linked immunosorbent assays (ELISAs). We found that all the groups had substantially high amounts of anti-TMEV total IgG titers, although the late group had a significantly lower amount of anti-TMEV total IgG titers (**, $p < 0.01$, ANOVA) compared with the early and control groups (Figure 9A). The number of anti-TMEV IgG1 titers was the least in the late group (Figure 9B); the number of anti-TMEV IgG2a titers was the highest in the early group (Figure 9C). We compared the IgG2a versus IgG1 ratios reflecting the T helper (Th) 1/Th2 balance among the three groups and found that the early and late groups had significantly higher ratios than the control group (**, $p < 0.01$, *, $p < 0.05$, ANOVA, Figure 9D).

2.8. Platelet Depletion Alters Lymphoproliferative Responses and Cytokine Production

In TMEV infection, the antiviral T cell responses can play either a beneficial role in viral clearance or a detrimental role in inflammatory demyelination [53]. We investigated whether platelet depletion could affect the lymphoproliferative responses to TMEV. We isolated mononuclear cells (MNCs) from the spleen of TMEV-infected mice and conducted lymphoproliferative assays using the Cell Counting Kit-8 (CCK-8). We found that the levels of anti-TMEV lymphoproliferative responses were comparable among the three groups (Supplemental Figure S8).

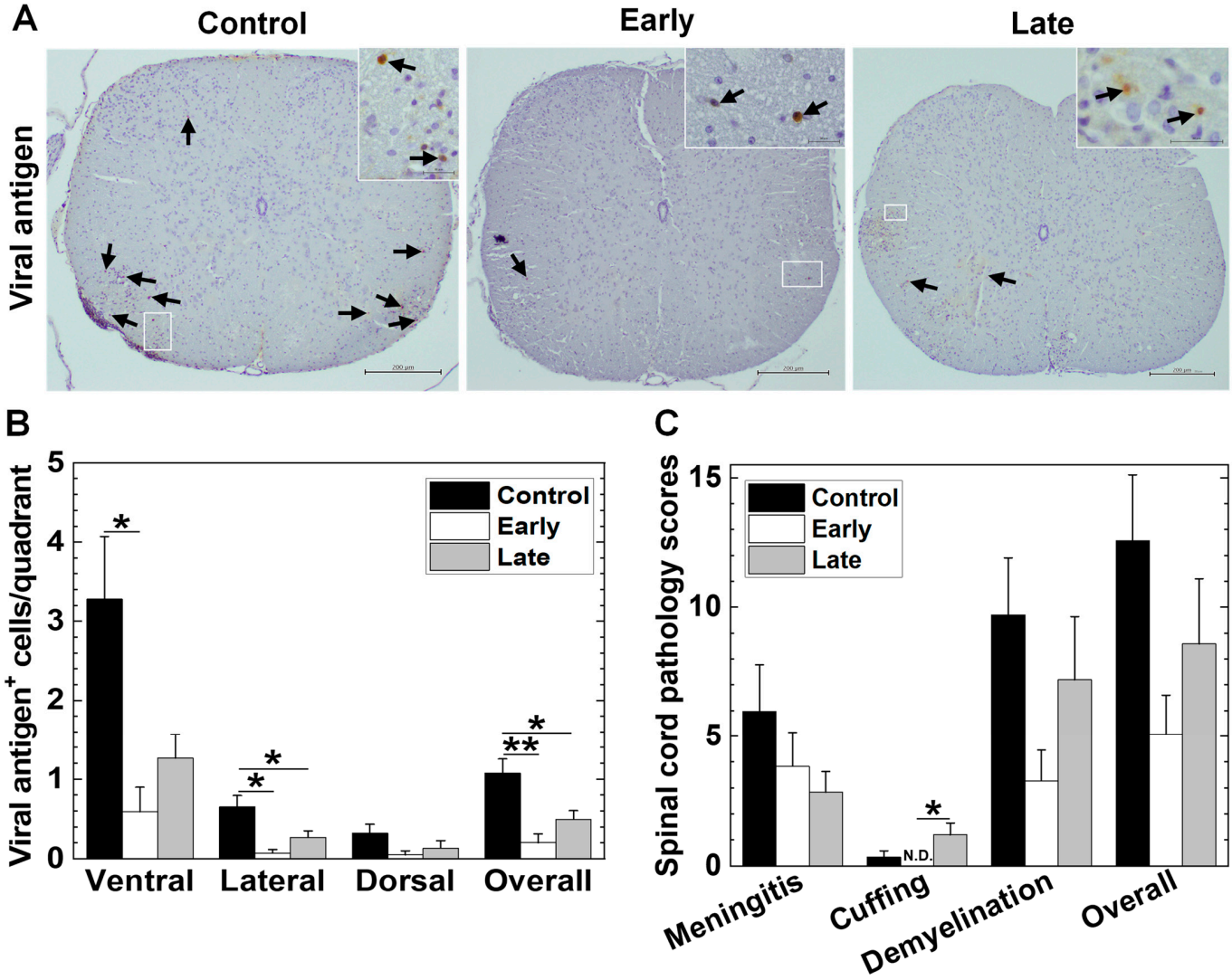

Figure 7. Immunohistochemistry against viral antigens in the spinal cord of TMEV-infected mice. We infected mice with TMEV, divided the mice into three groups, and intravenously injected them with a platelet-specific glycoprotein Ibα chain (GPIbα) depletion antibody 0 and 5 days p.i. (early group) or 18 and 22 days p.i. (late group), or with the control antibody (control group). (**A**) We found fewer viral antigen$^+$ cells (arrows) in the spinal cords of the early and late groups than in the control group. (**B**) Overall, we found significantly fewer viral antigen$^+$ cells in the early (**, $p < 0.01$, ANOVA) and late (* $p < 0.05$, ANOVA) groups than the control group. In the ventral funiculus, we detected a smaller number of viral antigen$^+$ cells in the early and late groups than in the control group. There was a statistical difference between the early and control groups (*, $p < 0.05$, ANOVA); the number of viral antigen$^+$ cells tended to be lower in the late group than in the control group ($p = 0.053$, ANOVA). We detected significantly fewer viral antigen$^+$ cells in the lateral funiculi of the early and late groups compared with the control group (*, $p < 0.05$, ANOVA). The spinal cord was divided into 12 to 13 transverse sections per mouse. (**C**) We quantified the pathological changes in the spinal cord using a spinal cord pathology scoring system. The levels of demyelination ($p = 0.098$, ANOVA) and overall pathology ($p = 0.088$, ANOVA) tended to be higher in the control group than in the early group, but not the late group. There were no differences in meningitis among the three groups, although the late group had higher scores of perivascular cuffing than the control ($p = 0.053$, ANOVA) and early (*, $p < 0.05$, ANOVA) groups. Each group was composed of five to fourteen mice. Results are the mean + standard error of the mean (SEM). Scale bar: (**A**), 200 μm; and inset, 20 μm. N.D., not detectable.

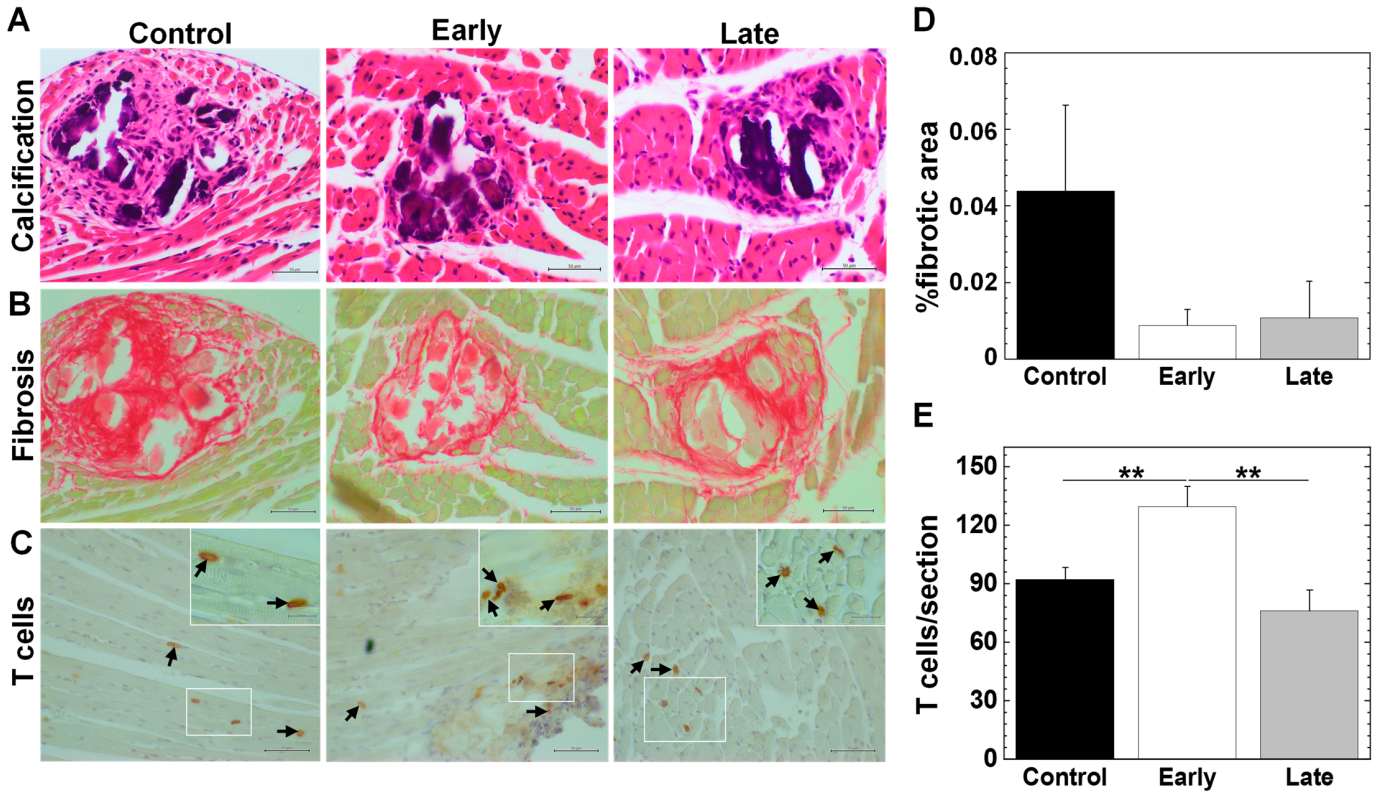

Figure 8. Cardiac pathology of TMEV-induced myocarditis. (**A**–**C**) We harvested the heart 35 days p.i. and dissected each heart into six to seven transverse sections. (**A**) Hematoxylin and eosin staining visualized calcification (dark purple). (**B**) Picrosirius red staining visualized fibrosis (red). (**C**) Immunohistochemistry against CD3 (T cell marker) showed $CD3^+$ T cell infiltration in the heart (arrows). (**D**) Although the control group had larger fibrotic areas, there were no statistical differences among the three groups. (**E**) The number of $CD3^+$ T cells in the heart was significantly higher in the early group than the control and late groups (**, $p < 0.01$, ANOVA). There were no statistical differences in $CD3^+$ T cells in the heart between the control and late groups. (**D**,**E**) We quantified %fibrotic areas and the number of $CD3^+$ T cells/heart section/mouse using ImageJ (version 1.53e). Values are the mean + SEM of five to fourteen mice per group. Scale bar: (**A**), 50 μm; (**B**), 50 μm; (**C**), 50 μm; and inset, 20 μm.

We also quantified their cytokine production using MNC culture supernatants stimulated with TMEV or a mitogen by ELISAs. In TMEV stimulation, we compared the concentrations of four cytokines among the three groups. We detected higher levels of IFN-γ production in the early and late groups compared with the control group, although no statistical differences were seen among the three groups. In the TMEV stimulation, the amounts of interleukin (IL)-10 were similar among the three groups; those of IL-17 and IL-4 were not detectable in the three groups (Figure 10A,B). On the other hand, for the mitogen stimulation, we detected similar levels of IL-17, IFN-γ, IL-4, and IL-10 concentrations among the three groups (Figure 10C,D).

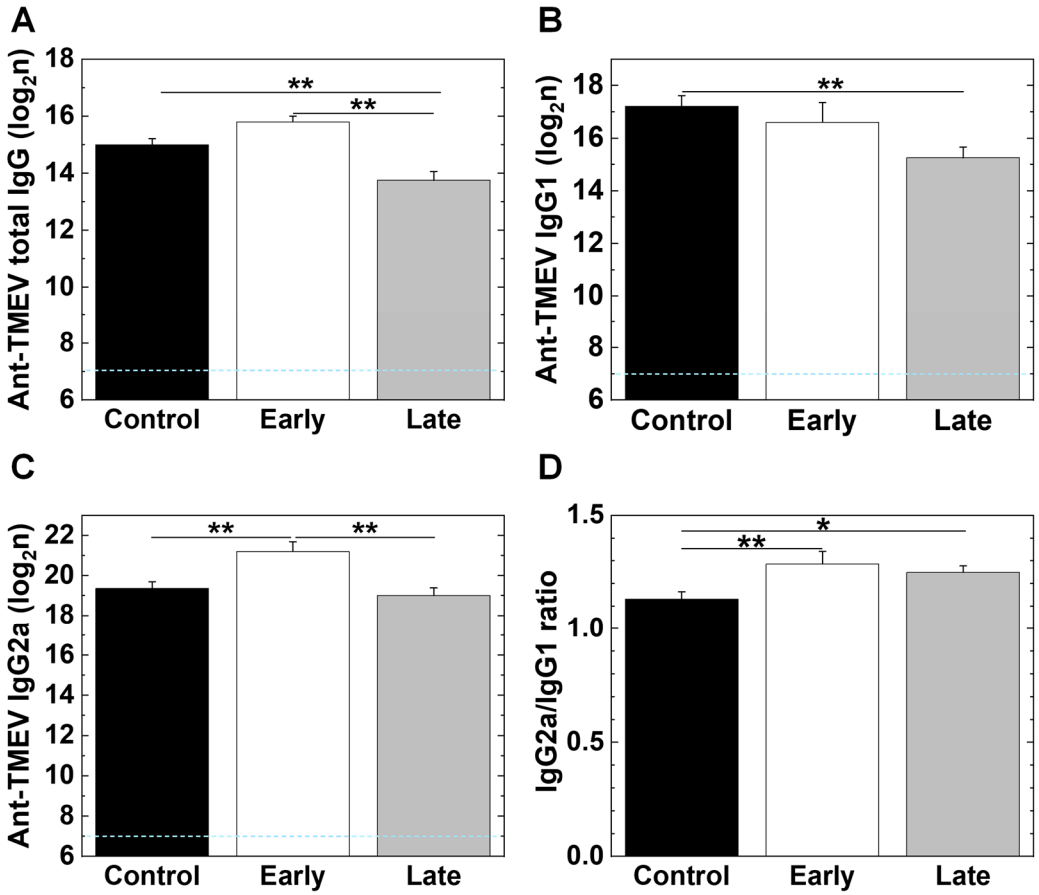

Figure 9. Anti-viral IgG isotype responses in TMEV-infected mice. We collected sera from the control, early, and late groups 35 days p.i. and compared anti-TMEV antibody titers (total IgG, IgG1, and IgG2a). The antibody titers were determined by enzyme-linked immunosorbent assays (ELISAs). (**A**) All groups had substantially high amounts of anti-TMEV IgG titers, although the control and early groups had significantly higher amounts of anti-TMEV total IgG titers (**, $p < 0.01$, ANOVA), compared with late group. (**B**) The number of anti-TMEV IgG1 titers was significantly lower in the late group than in the control group (**, $p < 0.01$, ANOVA). (**C**) Anti-TMEV IgG2a titers were significantly higher in the early group than in the late and control groups (**, $p < 0.01$, ANOVA). (**D**) The IgG2a versus IgG1 ratios, which reflect T helper (Th) 1/Th2 balance, were significantly higher in the early and late groups than in the control group (**, $p < 0.01$, *, $p < 0.05$, ANOVA). The IgG2a/IgG1 ratios were comparable between the early and late groups. Results are the mean + SEM of five to fourteen mice per group.

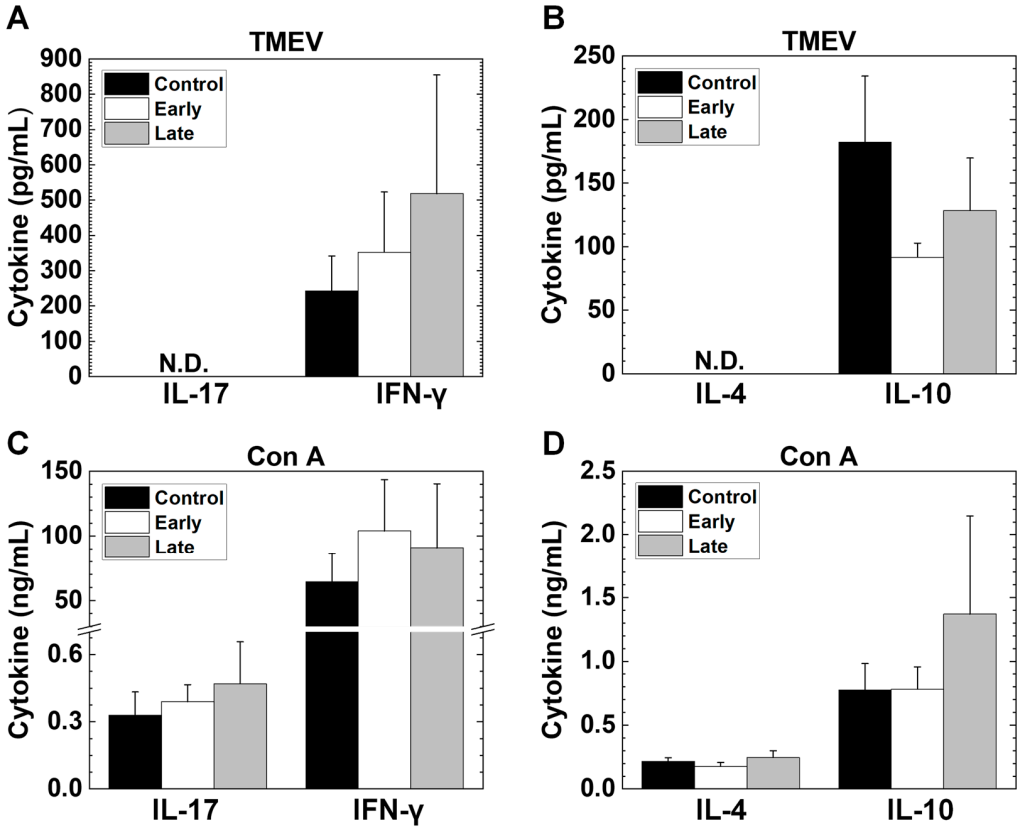

Figure 10. Cytokine production of splenic mononuclear cells (MNCs) from the control, early, and late groups. (**A**–**D**) Splenic MNCs were isolated from TMEV-infected mice and stimulated with TMEV (**A**,**B**) or a mitogen, concanavalin A (Con A) (**C**,**D**). The concentrations of interleukin (IL)-17, interferon (IFN)-γ, IL-4, and IL-10 in the culture supernatants were quantified by ELISAs. (**A**) There were no statistical differences in the concentrations of IFN-γ among the three groups, although the early and late groups had the higher levels of IFN-γ production than the control group in TMEV stimulation. (**B**) The concentrations of IL-10 were similar among the three groups. (**C**,**D**) The amounts of IL-17, IFN-γ, IL-4, and IL-10 were similar in response to Con A among the three groups. Results are the mean + SEM from two to six pools of spleens with two to three mice per group. N.D., not detectable.

3. Discussion

Platelets can bind and internalize various virions, including HIV, for viral clearance [54] or, in turn, can be utilized by viruses, including SARS-CoV-2 and dengue virus [55,56], to spread to various organs. Platelets have also been shown to play a beneficial or detrimental role in viral infections in various organs, including the CNS and heart by modulating immune responses [57,58]. In the current study, we aimed to clarify the role of platelets in TMEV infection, which has been used as a viral model for immune-mediated CNS and cardiac diseases, i.e., MS and myocarditis. TMEV has been shown to infect most cell types in vitro [59] and can cause viremia in vivo following experimental inoculation [7]. However, in vivo, TMEV can replicate efficiently only in limited cell types and organs (i.e., heart, skeletal muscle, intestine, and CNS); TMEV was eradicated by anti-viral immune responses by 2 weeks p.i. from the most organs except the CNS. In the CNS, TMEV initially infected neurons in the gray matter of the brain; later, TMEV persistently infected macrophages and glial cells in the white matter of the spinal cord. Although the viral receptor of TMEV has not been identified [60,61], in theory, platelets could contribute to viral clearance or spread to the organs, if TMEV can bind platelets. However, this was not the case in TMEV infection, since we did not detect the viral genomes from platelets isolated from the TMEV-infected mice at any time point (Supplemental Figure S2).

Besides virus–platelet binding, platelets have also been suggested to play diverse immunological roles, modulating viral infections and immune-mediated diseases of the CNS and heart, including MS [62–64], by various mechanisms. Platelets contain immune-related mRNAs and proteins and all molecular machinery, including ri-bosomes, to translate mRNA [65,66]. Thus, platelets can deliver, transfer, or express immune-related molecules/mRNAs from systemic circulation to various organs, interacting with various immune cells and vascular endothelial cells [67]. In TMEV infection, both humoral and cellular immune responses have been shown to contribute to viral clearance, although uncontrolled immune responses play a detrimental role, resulting in tissue damage in the CNS and heart. As reported in other viral infections, initially, TMEV infection induced innate immune responses followed by the induction of anti-viral T cell and antibody responses around 1 week p.i. and anti-viral antibodies and $CD4^+$ and $CD8^+$ T cells contributed to viral clearance in the brain and heart 2 weeks p.i. [68–70]. On the other hand, around 1 month p.i., the immune effectors play a detrimental role in TMEV-IDD or in fibrosis and cardiac remodeling in myocarditis.

In the current study, we conducted transcriptome analyses using spleen samples as a representative of lymphoid organs and found the upregulation of innate immune genes, including 2′-5′-oligoadenylate synthetases 2 (*Oas2*) and 1G (*Oas1g*) 4 and 7 days p.i., as well as distinct Ig- and TCR-related genes, including IgG heavy chain variable region (*Ighv*), *Ighg2c*, and *Igha*, 7 and 35 days p.i. (Figure 2). These results were consistent with the distinct roles of each immune effector during the time course of TMEV infection, as described previously [24,57,64,71]. In addition, using the DAVID functional clustering of DEGs in the spleen (Supplemental Table S2), we demonstrated that the enrichment scores of multiple immune-related pathways, including "immune system process," "defense response," "innate immune response," and "antigen processing and presentation," were high 4 and 7 days p.i. Furthermore, our PCA of the splenic transcriptome data showed that the overall gene expression profiles differed between the TMEV-infected and control mice (Figure 4A) as well as between the samples 4, 7, and 35 days p.i. (Supplemental Figure S3).

Unlike the spleen samples, the platelet transcriptome analyses using the DAVID showed that the enrichment scores of immune-related pathways were low (Supplemental Table S3); our PCA of the platelet transcriptomes did not separate the samples between the TMEV-infected versus control groups (Figure 4B), but separated the samples on days 4 and 7 versus the samples on day 35 (Figure 5A,C). Thus, in the platelets, immune-related gene expressions changed individually, but not in specific immune pathways, which did not alter the overall gene expression patterns. The overall platelet gene expression profile seemed to be influenced by aging; previously, age-related changes in the expression levels of various platelet mRNAs, including immune-related genes, have been reported in both mice and humans [72–79].

Although we did not determine how these individual immune gene expressions were changed in the platelets of the TMEV-infected mice, the gene expression changes were unlikely to be caused by direct virus infection in the platelets, since we did not detect the viral genome in the platelets at any time point (Supplemental Figure S2). We also did not determine the precise roles of individual platelet genes whose expressions changed over the course of TMEV infection. The following genes at each time point potentially could modulate anti-viral immunity as well as immunopathology: the upregulations of MHC class I-related genes and IFN-related genes 4 and 7 days p.i.; and the downregulations of distinct immune-related genes, including *Cd55*, 35 days p.i. For example, upregulated MHC class I (*H2-D1*, *H2-K1*) and β_2 microglobulin (*B2m*) genes on platelets could result in the modulation of anti-viral $CD8^+$ T cell responses, since platelets can present viral antigens to $CD8^+$ T cells in infections [80,81]. $CD8^+$ T cells have been shown to be protective, clearing virus-infected cells, or autoreactive, causing tissue damage in TMEV infection [82,83]. CD55, the decay-accelerating factor (DAF) complement, dissociates the C3 convertase, preventing the generation of C3a; the downregulation of CD55 could result in an exacerbation of inflammation. The regulation of inflammation by CD55 has been reported

in viral infections and immune-mediated diseases [84,85]. On the other hand, we found the upregulation of microtubule-related genes in cluster 7, including tubulin and dynein, 35 days p.i. Microtubules and microtubule-binding proteins, such as dynein and kinesins, play key roles in platelet shape changes (discoid to spherical), activation, and granule exocytosis [86–89]. In Supplemental Table S7, we demonstrated the upregulations of the microtubule-related genes, including tubulin (*Tubb2b*), dyneins (*Dnah2*, *Dnah6*, *Dnah7a*, *Dnah9*, and *Dnah17*), and kinesins (*Kif1a*, *Kif1b*, *Kif9*, *Kif16b*, *Kif21a*, *Kif26b*, and *Kifc3*). Although we do not know the functional relevance of these molecules and their interactions in TMEV infection, platelet activation and migration have been reported to depend on a series of changes in their dynamic cytoskeleton and morphology; for example, spherical platelets are transported more quickly to the vessel wall than disc-shaped platelets, giving them a better chance to adhere near the inflammatory site.

Histologically, we detected platelets in the CNS and hearts of the TEMV-infected mice. In the CNS, we found a small number of platelets attached to the luminal side of the vascular endothelia, adjacent to inflammatory lesions. The extent and localization of platelets in TMEV infection were similar to those in EAE, whose platelet accumulation has been reported previously [31]. In the hearts, platelet accumulations were more diffuse, independent of focal lesions. Since we found that the platelets did not infiltrate into the parenchyma of the inflammatory lesions in the CNS or heart, the platelets seemed to be indirectly involved in TMEV-IDD and myocarditis by modulating immune responses in the peripheral lymphoid organs. Platelets could also contribute to an exacerbation of inflammation, in which platelets bound to the luminal side of inflamed vessels, serving as a kind of "platform," recruit activated T cells, which could lead to an enhancement of T cell infiltration in the lesions [90].

The above platelet transcriptome analyses and histological detection of platelets in the CNS and heart suggested that platelets may contribute to viral clearance or immunopathology. Thus, we tested whether platelet depletion in TMEV infection could change the pathology of TMEV-IDD and myocarditis. We found that platelet depletion decreased the levels of viral persistence in the spinal cord (Figure 7A,B). Platelet depletion also ameliorated the neuropathology (demyelination and overall scores) in the spinal cord and fibrosis in the heart, although neither the CNS nor cardiac pathology scores reached a level of statistical significance compared with the controls (Figures 7C and 8). Our findings were consistent with the previous reports that platelet depletion has been demonstrated to ameliorate other immune-mediated disease models, including EAE [31,91–93].

We tested whether the decreased TMEV persistence in the CNS could be due to changes in anti-viral immune responses [94]. We found that both the platelet-depleted and control groups developed comparable anti-viral humoral and cellular immune responses, i.e., total anti-TMEV IgG titers and TMEV-specific lymphoproliferative responses, respectively (Figure 8A; Supplemental Figure S8). On the other hand, the platelet-depleted mice had the higher IgG2a/IgG1 ratios than the control mice. These changes in anti-TMEV IgG isotype responses were consistent with the higher production of IFN-γ (representative Th1 cytokine) [95] in the platelet-depleted groups than in the control group; Th1 and Th2 cytokines contribute to the isotype switching of IgG2a and IgG1 in mice, respectively [96]. In addition, IFN-γ itself has been shown to contribute to the clearance of various viruses, including TMEV [97–101]. In TMEV infection, IL-17-producing Th17 cells seemed to play a pathologic role, and IFN-γ-producing Th1 cells can be protective [4,9]. In contrast, in EAE models, both Th1 and Th17 cells have been demonstrated to be pathogenic, although there have been exceptions in some EAE models in which IFN-γ played a protective role [29].

Although our platelet depletion experiments suggested a potential detrimental role of platelets in TMEV-IDD and myocarditis, there were potential confounding findings in our experiments, which inevitably occurred in most platelet depletion/blocking experiments, in particular, bleeding. Since our anti-GPIbα antibody injections successfully depleted platelets, the platelet-depleted mice had severe anemia with low hemoglobin concentrations, reduced red blood cell counts, and fecal occult blood (Supplemental Figure S7) [102]; their

white blood cell counts were also decreased, although these did not reach a statistical difference. In addition, simultaneous platelet depletion and intracerebral viral inoculation resulted in significant body weight loss in the early group, in which 45% (5/9) of the mice died, likely due to brain hemorrhages. Thus, we were not able to refute that the reduced blood parameters as well as hemorrhage-associated stress might have affected the outcomes of our experiments. Moreover, our pilot experiments showed that more than two antibody injections per mouse often made platelet depletion less efficient, likely due to the generation of neutralizing anti-rat IgG, which meant only up to two antibody injections could be used to reproduce a substantial amount of platelet depletion. Thus, one should be cautious when evaluating the results of platelet depletion experiments similar to our experimental setting.

To address this concern, several platelet antagonists blocking the receptors on platelets can be used as candidates that inhibit platelet function without depleting platelets. For example, cangrelor is an inhibitor of platelet $P2Y_{12}$ receptor [103–105]; MRS2179 is a platelet $P2Y_1$ receptor antagonist [106,107]; and monoclonal antibody against platelet glycoprotein IIb/IIIa (GPIIb/IIIa) inhibits platelet aggregation [108], although these antagonists have been reported to increase the risk of bleeding. Rather than direct platelet inhibition at a single receptor, other anti-thrombotic agents, such as apyrase, have been reported to show the multimodal, indirect inhibition of platelets without increasing the risk of bleeding [109]. On the other hand, if a specific interaction between platelets and other cell types is proven to play a crucial role in the pathophysiology of MS and myocarditis in the future, blocking these interactions by the platelet receptor ligands on the non-platelet cells (e.g., vascular endothelia, T cells, or macrophages) [31] is another strategy to overcome these adverse events.

In conclusion, we demonstrated platelet involvement in TMEV infection; we found changes in platelet gene expressions as well as platelet attachment to the vessels adjacent to inflammatory lesions in the CNS and heart. Platelet depletion decreased viral persistence in the CNS, which was associated with altered anti-viral IgG isotype responses and IFN-γ production. Therefore, platelets can be a target in virus-induced CNS inflammatory diseases, possibly also in MS, as well as viral myocarditis.

4. Materials and Methods

4.1. Animal Experiments

We purchased four-week-old female SJL/J mice from Jackson Laboratory (Bar Harbor, ME, USA) and four-week-old male C3H/HeNJcl mice from CLEA Japan, Inc., (Tokyo, Japan). Mice were maintained under specific pathogen-free conditions in the animal care facility at Louisiana State University Health—Shreveport (LSUHS, Shreveport, LA, USA) or Kindai University Faculty of Medicine (Osaka, Japan). We inoculated five- to six-week-old mice intracerebrally (i.c) with 2×10^5 plaque forming units (PFUs) of the Daniels (DA) strain of TMEV [110]. Control mice were injected with phosphate-buffered saline (PBS). For transcriptome analyses, mice were killed 4, 7, and 35 days p.i., and platelet and spleen samples were harvested from TMEV-infected and control mice. We used five to seven mice/group/time point. All experimental procedures were approved by the Institutional Animal Care and Use Committee of LSUHS and Kindai University Faculty of Medicine and performed according to the criteria outlined by the National Institutes of Health (NIH) [111].

4.2. Platelet Isolation

Mouse blood was collected in the syringes prefilled with 0.1 mL of a citrate–dextrose solution (ACD, Sigma-Aldrich, Co., St Louis, MO, USA) by cannulation to the carotid artery [112]. Collected blood was centrifuged at $118\times$ *g* for 8 min to obtain platelet-rich plasma followed by platelet isolation with centrifugation at $735\times$ *g* for 10 min. Platelets were resuspended with PBS (pH 7.37–7.38) and stored at -80 °C until used.

4.3. RNA-Seq

Total RNA was isolated from platelets and the spleen using the RNeasy Mini Kit (Qiagen, Valencia, CA, USA) and TRIzol Reagent (Thermo Fisher Scientific Inc., Waltham, MA, USA), according to the manufacturers' instructions. DNase treatment was conducted using the RNase-Free DNase Set (Qiagen) as a part of RNA isolation. The purity of all samples was determined by the NanoDrop One/One^{c} Spectrophotometer (Thermo Fisher Scientific Inc.). RNA-seq was conducted by MR DNA (Shallowater, TX, USA) using a HiSeq system (Illumina, San Diego, CA, USA). Raw sequence (FASTQ) data were mapped by "Spliced Transcripts Alignment to a Reference (STAR)" and counted by the R version 4.2.3 [113] and the R packages, "GenomicAlignments" and "TxDb.Mmusculus.UCSC.mm10.ensGene." The data were normalized by the R package "TCC (Tag Count Comparison)" based on the "differentially expressed gene elimination strategy (DEGES)" [114]. The normalized read count data were converted to logarithmic data for further analyses. The FASTQ files and read count data were deposited into the GEO at the National Center for Biotechnology Information (NCBI, Bethesda, MD, USA; accession no. GSE253385, https://www.ncbi.nlm.nih.gov/geo/query/acc.cgi?acc=GSE253385 (accessed on 15 March 2024)).

4.4. Bioinformatics Analyses

Heat maps were used to visualize the expression patterns of the top 20 up- and downregulated genes in the spleen or platelets of TMEV-infected mice 4, 7, and 35 days p.i., respectively. We calculated the logarithmic ratio (log ratio) of TMEV-infected mice compared with control mice from the logarithmic read count data and created the heat maps using the R packages "gplots" and "genefilter" [71]. PCA was conducted as an unsupervised analysis to determine the similarities and differences among the samples, using the R program "prcomp" [24,115]. We created PCA graphs with 80% confidential ellipses, using the R packages "dplyr" and "ggplot2". Factor loadings were used to rank a set of genes contributing to the PCA distribution [116]. We conducted *k*-means clustering to categorize the genes based on their expression patterns throughout the disease's course using the R package "cclust" [24]. Davies–Bouldin indexes were calculated in the *k*-means clustering process to decide the optimum number of clusters [117]. A radar chart was drawn using the expression patterns of cluster centers [71]. To determine differentially expressed genes, we uploaded a list of ensemble gene IDs that were differentially expressed with $p < 0.05$, more than 2-fold up- or downregulated between the control and TMEV-infected groups to the DAVID (https://david.ncifcrf.gov/ (accessed on 15 March 2024)). The enrichment score was calculated using the Fisher's exact test, which compares the number of differentially expressed genes in the sample, matching with the total number of genes included in each canonical pathway.

4.5. Platelet Depletion In Vivo

To deplete platelets in vivo, we injected mice i.v. with an antibody against GPIbα (CD42b, #R300, Emfret Analytics, Eibelstadt, Germany) at a dose of 4 µg/g body weight. The control group received the control rat IgG (#C301, Emfret Analytics, Eibelstadt, Germany). The anti-GPIbα antibody depleted more than 95% of platelets in mice within 1 h after injection [118]. Antibody solutions were injected twice to each group on the following days p.i.: the early group, days 0 and 5; the late group, days 18 and 22; and the control group, days 0 and 5 or days 18 and 22. We monitored the body weight changes daily for 35 days.

4.6. Neuropathology and Cardiac Pathology

We killed mice 35 days p.i. with isoflurane (FUJIFILM Wako Pure Chemical Corporation, Osaka, Japan), harvested their sera, and perfused them with PBS extensively followed by a 4% paraformaldehyde (PFA, FUJIFILM Wako Pure Chemical Corporation) solution in PBS [119]. We harvested the CNS and heart and fixed them with a 4% PFA solution. The spinal cord was divided into 12 to 13 transverse segments and the heart was divided into

six to seven transverse slabs. We embedded the tissues in paraffin and made 4-µm-thick sections using the HM 325 Rotary Microtome (Thermo Fisher Scientific Inc. Osaka, Japan). We stained the CNS sections with Luxol fast blue (Solvent Blue 38; MP Biomedicals, LLC, Irvine, CA, USA) for myelin visualization and conducted neuropathological scoring of the spinal cords. We divided each spinal cord segment into four quadrants: the ventral funiculus, dorsal funiculus, and two lateral funiculi. Each funiculus containing meningitis, perivascular cuffing (inflammation), or demyelination was given a score of 1 in that pathological class. The total number of positive quadrants for each pathological class was determined and then divided by the total number of quadrants present on the slide and multiplied by 100 to obtain the percentage of involvement for each pathological class. An overall pathology score was also determined by recording a positive score if any pathology was seen in the quadrant and presented as the percentage of involvement [120]. For cardiac pathology, the heart sections were stained with hematoxylin (Sakura Finetek Japan Co., Ltd. Tokyo, Japan) and eosin (Thermo Fisher Scientific Inc.) for inflammation and calcification or picrosirius red (ScyTek Laboratories, Inc., Logan, UT, USA) for fibrosis. We analyzed the sections stained with picrosirius red to quantify the fibrotic areas by ImageJ (ImageJ, Wayne Rasband and contributors, NIH, USA, http://imagej.nih.gov/ij)) with a color threshold tool and a measure tool. The fibrotic area (mm^2) was used to calculate % fibrotic area, using the following formula:

$$\%\text{fibrotic area} = \frac{\text{fibrotic area}}{\text{fibrotic area} + \text{non fibrotic area}} \times 100$$

4.7. Immunohistochemistry

We visualized platelets, TMEV antigen$^+$ cells, and T cells by immunohistochemistry using anti-bodies against GPIbα/CD42b (100-fold dilution, Abcam, Tokyo, Japan) and integrin β3 [platelet glycoprotein IIIa (GPIIIa/CD61), 500-fold dilution, Cell Signaling Technology, Inc., Tokyo, Japan], anti-TMEV antibody [121], and anti-CD3 antibody (T cell marker, 120-fold dilution, Biocare Medical, Pacheco, CA, USA). For GPIbα and integrin β3 immunostaining, the CNS, heart, and spleen sections were pretreated with a 10 mM citrate buffer at a pH of 6.0 (Agilent Technologies Japan, Ltd., Tokyo, Japan) for 15 min at 95 °C using an MI-77 temperature-controllable microwave (Azumaya Medical Devices Inc., Tokyo, Japan) for antigen retrieval. For CD3 immunostaining, the CNS and heart sections were pretreated with a 10 mM citrate buffer at a pH of 6.0 (Agilent Technologies Japan, Ltd.) for 15 min at 120 °C using an autoclave [120]. The antibody/antigen complexes were visualized by a secondary antibody Histofine MAX-PO kit (Nichirei Biosciences Inc., Tokyo, Japan) with a 3,3′-diaminobenzidine (DAB, FUJIFILM Wako Pure Chemical Corporation) substrate solution. To quantify the levels of viral persistence in the spinal cord, we divided each spinal cord segment into four quadrants: the ventral funiculus, dorsal funiculus, and the two lateral funiculi, and we counted the number of TMEV antigen$^+$ cells in each quadrant of the spinal cord under a light microscope using a 10× objective lens. We quantified TMEV antigen+ cells using 12 to 13 spinal cord segments per mouse. To quantify T cell infiltration of the heart, we counted CD3$^+$ cells in all six to seven transverse slabs of the heart per mouse.

4.8. Anti-TMEV Isotype Antibody ELISAs

We collected blood from the heart 35 days p.i. and centrifuged the blood at 2775× g at 4 °C for 20 min. We used sera to assess the levels of anti-TMEV antibodies by ELISAs. We coated 96-well flat-bottom Nunc-Immuno plates (Thermo Fisher Scientific Inc.) with 10 µg/mL of purified TMEV antigens. After blocking the plates with 10% fetal bovine serum (FBS) and 0.2% Tween^{TM} 20 (Thermo Fisher Scientific Inc.) in PBS, we diluted the serum samples with the blocking solution by serial two-fold dilutions from 2^7 to 2^{28}, added the diluted serum samples to the plates, and incubated the plates at room temperature (RT) for 75 min. We washed the plates with a washing buffer consisting of 0.2% Tween^{TM} 20 in PBS and added horseradish peroxidase (HRP)-conjugated anti-mouse IgG (H+L) (2000-fold

dilution, Thermo Fisher Scientific Inc.), anti-mouse IgG1 (4000-fold dilution, Thermo Fisher Scientific Inc.), or anti-mouse IgG2a (4000-fold dilution, Southern Biotechnology Associates, Inc., Birmingham, AL, USA) secondary antibodies to the plates. After 90 min of incubation, we detected the immunoreactive complexes using the BD OptEIA™ TMB Substrate Reagent Set (BD Biosciences, San Jose, CA, USA) according to the manufacturer's instruction. The absorbances were measured at 450 nm using the Synergy H1 Hybrid Multi-Mode Microplate Reader (Agilent Technologies, Inc., Santa Clara, CA, USA). The anti-TMEV antibody titers was determined as the highest reciprocal of the dilution that had an absorbance higher than the average plus two standard deviations of naïve serum samples at a dilution of 2^7-fold.

4.9. Lymphoproliferative Responses and Cytokine ELISAs

We harvested the spleens from the early, late and control mice 35 days p.i. To make single-cell suspensions, we mashed the spleens on a metal mesh with 50 μm pores using the plunger of a 5 mL syringe and isolated MNCs using Histopaque®-1083 (Sigma-Aldrich, Co.). The splenic MNCs were cultured in RPMI-1640 medium (Sigma-Aldrich, Co.) supplemented with 10% FBS (Sigma-Aldrich, Co.), 2 mM L-glutamine (Sigma-Aldrich, Co.), 50 mM β-mercaptoethanol (FUJIFILM Wako Pure Chemical Corporation), and 1% antibiotics (Thermo Fisher Scientific Inc.) at 2×10^5 cells/well in 96-well plates (Sumitomo Bakelite Co., Ltd., Tokyo, Japan). We incubated the MNCs with or without 1 μg purified TMEV antigens at 37 °C with 5% CO_2 for 5 days. To assess the levels of TMEV-specific lymphoproliferative responses, we added 3 μL/well of a CCK-8 solution (Dojindo Laboratories, Kumamoto, Japan) in the cell culture system for the last 24 h. All cultures were performed in triplicate and the absorbances were measured at 450 nm using the Synergy H1 Hybrid Multi-Mode Microplate Reader. The data are expressed as stimulation indexes: (mean absorbance of the wells stimulated with TMEV antigen)/(mean absorbance of wells without stimulation). For cytokine ELISAs, we cultured the splenic MNCs at 8×10^6 cells/well in 6-well plates, stimulated the splenic MNCs with 8×10^6 PFUs of TMEV (multiplicity of infection of 1) or 10 μg/mL of ConA (Sigma-Aldrich, Co.), and incubated the plates at 37 °C with 5% CO_2 for 2 days. The culture supernatants were collected and stored at −80 °C until examined. The concentrations of IL-17A (BioLegend, Inc., San Diego, CA, USA), IFN-γ, IL-4, and IL-10 (BD Biosciences, San Jose, CA, USA) were quantified in the culture in duplicate wells using ELISA kits, according to the manufacturers' instructions [120].

4.10. Statistics

Statistical analyses were conducted using OrigenPro 2023 (OrigenLab, Corporation, Northampton, MA). We conducted Student's *t*-test for two groups and analysis of variance (ANOVA) with Fisher's post hoc LSD test for three or more groups. $p < 0.05$ was considered to indicate a significant difference.

Supplementary Materials: The following supporting information can be downloaded at: https://www.mdpi.com/article/10.3390/ijms25063460/s1.

Author Contributions: I.T. conceived of and supervised the project. I.T., S.O., F.S., F.N.E.G., H.T. and M.Y.K. designed the experiments. I.A., S.O., F.S., S.K. and A.-M.P. conducted the experiments. I.A. and S.O. conducted the bioinformatics analyses. I.A., S.O., F.S. and I.T. wrote the manuscript. All authors contributed to the article and approved the submitted version. All authors have read and agreed to the published version of the manuscript.

Funding: This work is supported by the Ministry of Education, Culture, Sports, Science and Technology, Japan, through the Monbukagakusho (MEXT, 2021-2025) Scholarship (I.A.), Grant-in Aid for Scientific Research KAKENHI from the Japan Society for the Promotion of Science (JSPS) (JP22K07527 (S.O.), JP23K06493 (F.S.), JP21K07167 (H.T.), and JP22K18378 and JP23K08901 (I.T.)), Novartis Pharma Research Grants (S.O. and I.T.), the Royal Society Wolfson Foundation (RSWF\R3\183001, (F.N.E.G.)), the Hokkaido Lawyer Association for Hepatitis B (Orange funding) (H.T.), and Hokkaido Organization for Translational Research (A seeds) (H.T.).

Institutional Review Board Statement: All animal experiments were approved by the Kindai University Faculty of Medicine (Osaka, Japan) Institutional Animal Care and Use Committee (KAME-2022-001, 08 March 2022) and LSUHS (P-14-027, 20 May 2014).

Informed Consent Statement: Not applicable.

Data Availability Statement: The data generated for this study can be found in the GEO at the NCBI (accession no. GSE253385, https://www.ncbi.nlm.nih.gov/geo/query/acc.cgi?acc=GSE253385 (accessed on 15 March 2024)).

Acknowledgments: We would like to express our gratitude to the following members of the Department of Microbiology, Kindai University Faculty of Medicine: Cong Thanh Nguyen, Kota Moriguchi, Reona Shiro, Namie Sakiyama, Yoshiko Ito, Koya Mineta, Toshiki Izumi, and the late Toshinori Nakayama, President of Chiba University, Chiba, Japan.

Conflicts of Interest: The authors declare no conflicts of interest.

References

1. Flint, S.J.; Racaniello, V.R.; Rall, G.F.; Hatziioannou, T.; Skalka, A.M. Patterns and pathogenesis. In *Principles of Virology, Volume 2: Pathogenesis and Control*, 5th ed.; Flint, S.J., Racaniello, V.R., Rall, G.F., Hatziioannou, T., Skalka, A.M., Eds.; ASM Press: Washington, DC, USA, 2020; pp. 146–186.
2. Fairweather, D.; Rose, N.R. Coxsackievirus-induced myocarditis in mice: A model of autoimmune disease for studying immunotoxicity. *Methods* **2007**, *41*, 118–122. [CrossRef] [PubMed]
3. Liu, J.; Li, Y.; Liu, Q.; Yao, Q.; Wang, X.; Zhang, H.; Chen, R.; Ren, L.; Min, J.; Deng, F.; et al. SARS-CoV-2 cell tropism and multiorgan infection. *Cell Discov.* **2021**, *7*, 17. [CrossRef]
4. Sato, F.; Tanaka, H.; Hasanovic, F.; Tsunoda, I. Theiler's virus infection: Pathophysiology of demyelination and neurodegeneration. *Pathophysiology* **2011**, *18*, 31–41. [CrossRef] [PubMed]
5. Theiler, M.; Gard, S. Encephalomyelitis of mice: I. Characteristics and pathogenesis of the virus. *J. Exp. Med.* **1940**, *72*, 49–67. [CrossRef] [PubMed]
6. DePaula-Silva, A.B. The contribution of microglia and brain-infiltrating macrophages to the pathogenesis of neuroinflammatory and neurodegenerative diseases during TMEV infection of the central nervous system. *Viruses* **2024**, *16*, 119. [CrossRef]
7. Tsunoda, I.; McCright, I.J.; Kuang, L.-Q.; Zurbriggen, A.; Fujinami, R.S. Hydrocephalus in mice infected with a Theiler's murine encephalomyelitis virus variant. *J. Neuropathol. Exp. Neurol.* **1997**, *56*, 1302–1313. [CrossRef] [PubMed]
8. Tsunoda, I.; Kurtz, C.I.B.; Fujinami, R.S. Apoptosis in acute and chronic central nervous system disease induced by Theiler's murine encephalomyelitis virus. *Virology* **1997**, *228*, 388–393. [CrossRef]
9. Oleszak, E.L.; Chang, J.R.; Friedman, H.; Katsetos, C.D.; Platsoucas, C.D. Theiler's virus infection: A model for multiple sclerosis. *Clin. Microbiol. Rev.* **2004**, *17*, 174–207. [CrossRef]
10. Tsunoda, I.; Kuang, L.-Q.; Fujinami, R.S. Induction of autoreactive $CD8^+$ cytotoxic T cells during Theiler's murine encephalomyelitis virus infection: Implications for autoimmunity. *J. Virol.* **2002**, *76*, 12834–12844. [CrossRef]
11. Kriesel, J.D.; White, A.; Hayden, F.G.; Spruance, S.L.; Petajan, J. Multiple sclerosis attacks are associated with picornavirus infections. *Mult. Scler.* **2004**, *10*, 145–148. [CrossRef]
12. Ascherio, A. Environmental factors in multiple sclerosis. *Expert. Rev. Neurother.* **2013**, *13*, 3–9. [CrossRef]
13. Lünemann, J.D.; Münz, C. EBV in MS: Guilty by association? *Trends Immunol.* **2009**, *30*, 243–248. [CrossRef]
14. Sato, F.; Omura, S.; Kawai, E.; Martinez, N.E.; Acharya, M.M.; Reddy, P.C.; Chaitanya, G.V.; Alexander, J.S.; Tsunoda, I. Distinct kinetics of viral replication, T cell infiltration, and fibrosis in three phases of myocarditis following Theiler's virus infection. *Cell Immunol.* **2014**, *292*, 85–93. [CrossRef]
15. Goetzke, C.C.; Althof, N.; Neumaier, H.L.; Heuser, A.; Kaya, Z.; Kespohl, M.; Klingel, K.; Beling, A. Mitigated viral myocarditis in A/J mice by the immunoproteasome inhibitor ONX 0914 depends on inhibition of systemic inflammatory responses in CoxsackievirusB3 infection. *Basic Res. Cardiol.* **2021**, *116*, 7. [CrossRef]
16. Global Burden of Disease Study 2013 Collaborators. Global, regional, and national incidence, prevalence, and years lived with disability for 301 acute and chronic diseases and injuries in 188 countries, 1990-2013: A systematic analysis for the Global Burden of Disease Study 2013. *Lancet* **2015**, *386*, 743–800. [CrossRef] [PubMed]
17. Cooper, L.T., Jr. Myocarditis. *N. Engl. J. Med.* **2009**, *360*, 1526–1538. [CrossRef] [PubMed]
18. Huber, S.A.; Gauntt, C.J.; Sakkinen, P. Enteroviruses and myocarditis: Viral pathogenesis through replication, cytokine induction, and immunopathogenicity. *Adv. Virus Res.* **1998**, *51*, 35–80. [CrossRef] [PubMed]
19. Ali, M.; Shiwani, H.A.; Elfaki, M.Y.; Hamid, M.; Pharithi, R.; Kamgang, R.; Egom, C.B.; Oyono, J.L.E.; Egom, E.E.-A. COVID-19 and myocarditis: A review of literature. *Egypt. Heart J.* **2022**, *74*, 23. [CrossRef] [PubMed]
20. Fairweather, D.; Stafford, K.A.; Sung, Y.K. Update on coxsackievirus B3 myocarditis. *Curr. Opin. Rheumatol.* **2012**, *24*, 401–407. [CrossRef] [PubMed]
21. Liu, P.P.; Mason, J.W. Advances in the understanding of myocarditis. *Circulation* **2001**, *104*, 1076–1082. [CrossRef]

22. Gómez, R.M.; Rinehart, J.E.; Wollmann, R.; Roos, R.P. Theiler's murine encephalomyelitis virus-induced cardiac and skeletal muscle disease. *J. Virol.* **1996**, *70*, 8926–8933. [CrossRef]
23. Rames, D.S. *The Etiopathogenesis of Theiler's Murine Encephalomyelitis Virus (TMEV)-Induced Cardiomyopathy, Including Characterization of New Strains of TMEV*; Texas A&M University: College Station, TX, USA, 1995.
24. Omura, S.; Kawai, E.; Sato, F.; Martinez, N.E.; Chaitanya, G.V.; Rollyson, P.A.; Cvek, U.; Trutschl, M.; Alexander, J.S.; Tsunoda, I. Bioinformatics multivariate analysis determined a set of phase-specific biomarker candidates in a novel mouse model for viral myocarditis. *Circ. Cardiovasc. Genet.* **2014**, *7*, 444–454. [CrossRef]
25. Omura, S.; Tsunoda, I. Cutting-edge research about phathomechanisms of multiple sclerosis. *Pharma Medica* **2021**, *39*, 67–71.
26. Mehmood, A.; Song, S.; Du, X.; Yan, H.; Wang, X.; Guo, L.; Li, B. mRNA expression profile reveals differentially expressed genes in splenocytes of experimental autoimmune encephalomyelitis model. *Int. J. Exp. Pathol.* **2023**, *104*, 247–257. [CrossRef]
27. Vögtle, T.; Sharma, S.; Mori, J.; Nagy, Z.; Semeniak, D.; Scandola, C.; Geer, M.J.; Smith, C.W.; Lane, J.; Pollack, S.; et al. Heparan sulfates are critical regulators of the inhibitory megakaryocyte-platelet receptor G6b-B. *Elife* **2019**, *8*, e46840. [CrossRef]
28. Liu, Z.; Li, L.; Zhang, H.; Pang, X.; Qiu, Z.; Xiang, Q.; Cui, Y. Platelet factor 4(PF4) and its multiple roles in diseases. *Blood Rev.* **2023**, *64*, 101155. [CrossRef]
29. Omura, S.; Sato, F.; Martinez, N.E.; Park, A.-M.; Fujita, M.; Kennett, N.J.; Cvek, U.; Minagar, A.; Alexander, J.S.; Tsunoda, I. Bioinformatics analyses determined the distinct CNS and peripheral surrogate biomarker candidates between two mouse models for progressive multiple sclerosis. *Front. Immunol.* **2019**, *10*, 516. [CrossRef] [PubMed]
30. Jeimy, S.B.; Tasneem, S.; Cramer, E.M.; Hayward, C.P.M. Multimerin 1. *Platelets* **2008**, *19*, 83–95. [CrossRef] [PubMed]
31. Langer, H.F.; Choi, E.Y.; Zhou, H.; Schleicher, R.; Chung, K.-J.; Tang, Z.; Göbel, K.; Bdeir, K.; Chatzigeorgiou, A.; Wong, C.; et al. Platelets contribute to the pathogenesis of experimental autoimmune encephalomyelitis. *Circ. Res.* **2012**, *110*, 1202–1210. [CrossRef] [PubMed]
32. Schrottmaier, W.C.; Schmuckenschlager, A.; Pirabe, A.; Assinger, A. Platelets in viral infections—Brave soldiers or trojan horses. *Front. Immunol.* **2022**, *13*, 856713. [CrossRef] [PubMed]
33. Terada, H.; Baldini, M.; Ebbe, S.; Madoff, M.A. Interaction of influenza virus with blood platelets. *Blood* **1966**, *28*, 213–228. [CrossRef]
34. Page, M.J.; Pretorius, E. A champion of host defense: A generic large-scale cause for platelet dysfunction and depletion in infection. *Semin. Thromb. Hemost.* **2020**, *46*, 302–319. [CrossRef]
35. Youssefian, T.; Drouin, A.; Massé, J.-M.; Guichard, J.; Cramer, E.M. Host defense role of platelets: Engulfment of HIV and *Staphylococcus aureus* occurs in a specific subcellular compartment and is enhanced by platelet activation. *Blood* **2002**, *99*, 4021–4029. [CrossRef]
36. Flaujac, C.; Boukour, S.; Cramer-Bordé, E. Platelets and viruses: An ambivalent relationship. *Cell Mol. Life Sci.* **2010**, *67*, 545–556. [CrossRef] [PubMed]
37. Zahn, A.; Jennings, N.; Ouwehand, W.H.; Allain, J.-P. Hepatitis C virus interacts with human platelet glycoprotein VI. *J. Gen. Virol.* **2006**, *87*, 2243–2251. [CrossRef] [PubMed]
38. Chabert, A.; Hamzeh-Cognasse, H.; Pozzetto, B.; Cognasse, F.; Schattner, M.; Gomez, R.M.; Garraud, O. Human platelets and their capacity of binding viruses: Meaning and challenges? *BMC Immunol.* **2015**, *16*, 26. [CrossRef]
39. Negrotto, S.; Jaquenod de Giusti, C.; Rivadeneyra, L.; Ure, A.E.; Mena, H.A.; Schattner, M.; Gomez, R.M. Platelets interact with Coxsackieviruses B and have a critical role in the pathogenesis of virus-induced myocarditis. *J. Thromb. Haemost.* **2015**, *13*, 271–282. [CrossRef]
40. Elzey, B.D.; Tian, J.; Jensen, R.J.; Swanson, A.K.; Lees, J.R.; Lentz, S.R.; Stein, C.S.; Nieswandt, B.; Wang, Y.; Davidson, B.L.; et al. Platelet-mediated modulation of adaptive immunity: A communication link between innate and adaptive immune compartments. *Immunity* **2003**, *19*, 9–19. [CrossRef] [PubMed]
41. Italiano, J.E., Jr.; Shivdasani, R.A. Megakaryocytes and beyond: The birth of platelets. *J. Thromb. Haemost.* **2003**, *1*, 1174–1182. [CrossRef] [PubMed]
42. Smyth, S.S.; McEver, R.P.; Weyrich, A.S.; Morrell, C.N.; Hoffman, M.R.; Arepally, G.M.; French, P.A.; Dauerman, H.L.; Becker, R.C.; 2009 Platelet Colloquium Participants. Platelet functions beyond hemostasis. *J. Thromb. Haemost.* **2009**, *7*, 1759–1766. [CrossRef] [PubMed]
43. Herter, J.M.; Rossaint, J.; Zarbock, A. Platelets in inflammation and immunity. *J. Thromb. Haemost.* **2014**, *12*, 1764–1775. [CrossRef]
44. Jenne, C.N.; Urrutia, R.; Kubes, P. Platelets: Bridging hemostasis, inflammation, and immunity. *Int. J. Lab. Hematol.* **2013**, *35*, 254–261. [CrossRef] [PubMed]
45. Pulavendran, S.; Rudd, J.M.; Maram, P.; Thomas, P.G.; Akhilesh, R.; Malayer, J.R.; Chow, V.T.K.; Teluguakula, N. Combination therapy targeting platelet activation and virus replication protects mice against lethal influenza pneumonia. *Am. J. Respir. Cell Mol. Biol.* **2019**, *61*, 689–701. [CrossRef] [PubMed]
46. Lê, V.B.; Schneider, J.G.; Boergeling, Y.; Berri, F.; Ducatez, M.; Guerin, J.-L.; Adrian, I.; Errazuriz-Cerda, E.; Frasquilho, S.; Antunes, L.; et al. Platelet activation and aggregation promote lung inflammation and influenza virus pathogenesis. *Am. J. Respir. Crit. Care Med.* **2015**, *191*, 804–819. [CrossRef]
47. Ohtsuka, M.; Inoko, H.; Kulski, J.K.; Yoshimura, S. Major histocompatibility complex (Mhc) class Ib gene duplications, organization and expression patterns in mouse strain C57BL/6. *BMC Genom.* **2008**, *9*, 178. [CrossRef] [PubMed]

48. White, J.G.; Rao, G.H. Microtubule coils versus the surface membrane cytoskeleton in maintenance and restoration of platelet discoid shape. *Am. J. Pathol.* **1998**, *152*, 597–609. [PubMed]
49. Marek, I.; Hilgers, K.F.; Rascher, W.; Woelfle, J.; Hartner, A. A role for the alpha-8 integrin chain (itga8) in glomerular homeostasis of the kidney. *Mol. Cell Pediatr.* **2020**, *7*, 13. [CrossRef] [PubMed]
50. Hridi, S.U.; Barbour, M.; Wilson, C.; Franssen, A.J.P.M.; Harte, T.; Bushell, T.J.; Jiang, H.-R. Increased levels of IL-16 in the central nervous system during neuroinflammation are associated with infiltrating immune cells and resident glial cells. *Biology* **2021**, *10*, 472. [CrossRef]
51. Tanaka, H.; Horioka, K.; Yamamoto, M.; Asari, M.; Okuda, K.; Yamazaki, K.; Shimizu, K.; Ogawa, K. Overproduction of thrombopoietin by BRAFV600E-mutated mouse hepatocytes and contribution of thrombopoietin to hepatocarcinogenesis. *Cancer Sci.* **2019**, *110*, 2748–2759. [CrossRef]
52. Tsunoda, I.; Tolley, N.D.; Theil, D.J.; Whitton, J.L.; Kobayashi, H.; Fujinami, R.S. Exacerbation of viral and autoimmune animal models for multiple sclerosis by bacterial DNA. *Brain Pathol.* **1999**, *9*, 481–493. [CrossRef]
53. Tsunoda, I.; Iwasaki, Y.; Terunuma, H.; Sako, K.; Ohara, Y. A comparative study of acute and chronic diseases induced by two subgroups of Theiler's murine encephalomyelitis virus. *Acta Neuropathol.* **1996**, *91*, 595–602. [CrossRef]
54. Zucker-Franklin, D.; Seremetis, S.; Zheng, Z.Y. Internalization of human immunodeficiency virus type I and other retroviruses by megakaryocytes and platelets. *Blood* **1990**, *75*, 1920–1923. [CrossRef] [PubMed]
55. Barrett, T.J.; Bilaloglu, S.; Cornwell, M.; Burgess, H.M.; Virginio, V.W.; Drenkova, K.; Ibrahim, H.; Yuriditsky, E.; Aphinyanaphongs, Y.; Lifshitz, M.; et al. Platelets contribute to disease severity in COVID-19. *J. Thromb. Haemost.* **2021**, *19*, 3139–3153. [CrossRef] [PubMed]
56. Trugilho, M.R.d.; Hottz, E.D.; Brunoro, G.V.F.; Teixeira-Ferreira, A.; Carvalho, P.C.; Salazar, G.A.; Zimmerman, G.A.; Bozza, F.A.; Bozza, P.T.; Perales, J. Platelet proteome reveals novel pathways of platelet activation and platelet-mediated immunoregulation in dengue. *PLoS Pathog.* **2017**, *13*, e1006385. [CrossRef]
57. Kopeikina, E.; Ponomarev, E.D. The role of platelets in the stimulation of neuronal synaptic plasticity, electric activity, and oxidative phosphorylation: Possibilities for new therapy of neurodegenerative diseases. *Front. Cell Neurosci.* **2021**, *15*, 680126. [CrossRef] [PubMed]
58. Maier, A.; Braig, M.; Jakob, K.; Bienert, T.; Schäper, M.; Merkle, A.; Wadle, C.; Menza, M.; Neudorfer, I.; Bojti, I.; et al. Molecular magnetic resonance imaging of activated platelets allows noninvasive detection of early myocarditis in mice. *Sci. Rep.* **2020**, *10*, 13211. [CrossRef] [PubMed]
59. McCright, I.J.; Fujinami, R.S. Lack of correlation of Theiler's virus binding to cells with infection. *J. Neurovirol.* **1997**, *3* (Suppl. S1), S68–S70. [PubMed]
60. Takeda, K.; Kaifu, T.; Michihata, R.; Kinugawa, N.; Fujioka, A.; Tateno, A.; Toshima, K.; Kanoh, H.; Inamori, K.; Kamijo, K.; et al. Chronic encephalomyelitis virus exhibits cellular tropism and evades pDCs by binding to sialylated integrins as the cell surface receptors. *Eur. J. Immunol.* **2023**, *53*, e2350452. [CrossRef]
61. Lipton, H.L.; Kumar, A.S.M.; Hertzler, S.; Reddi, H.V. Differential usage of carbohydrate co-receptors influences cellular tropism of Theiler's murine encephalomyelitis virus infection of the central nervous system. *Glycoconj. J.* **2006**, *23*, 39–49. [CrossRef]
62. Orian, J.M.; D'Souza, C.S.; Kocovski, P.; Krippner, G.; Hale, M.W.; Wang, X.; Peter, K. Platelets in multiple sclerosis: Early and central mediators of inflammation and neurodegeneration and attractive targets for molecular imaging and site-directed therapy. *Front. Immunol.* **2021**, *12*, 620963. [CrossRef]
63. Saluk-Bijak, J.; Dziedzic, A.; Bijak, M. Pro-thrombotic activity of blood platelets in multiple sclerosis. *Cells* **2019**, *8*, 110. [CrossRef]
64. Krishnamurti, C.; Peat, R.A.; Cutting, M.A.; Rothwell, S.W. Platelet adhesion to dengue-2 virus-infected endothelial cells. *Am. J. Trop. Med. Hyg.* **2002**, *66*, 435–441. [CrossRef]
65. Kapur, R.; Zufferey, A.; Boilard, E.; Semple, J.W. Nouvelle cuisine: Platelets served with inflammation. *J. Immunol.* **2015**, *194*, 5579–5587. [CrossRef]
66. Rowley, J.W.; Schwertz, H.; Weyrich, A.S. Platelet mRNA: The meaning behind the message. *Curr. Opin. Hematol.* **2012**, *19*, 385–391. [CrossRef] [PubMed]
67. Gawaz, M. Platelets and inflammation. In *Platelet Function: Assessment, Diagnosis, and Treatment*, 1st ed.; Quinn, M., Fitzgerald, D., Eds.; Humana Press: Totowa, NJ, USA, 2005; pp. 115–147.
68. Olson, J.K. Effect of the innate immune response on development of Theiler's murine encephalomyelitis virus-induced demyelinating disease. *J. Neurovirol.* **2014**, *20*, 427–436. [CrossRef] [PubMed]
69. Olson, J.K.; Miller, S.D. The role of T cells and the innate immune system in the pathogenesis of Theiler's virus demyelinating disease. In *Experimental Models of Multiple Sclerosis*, 1st ed.; Lavi, E., Constantinescu, C.S., Eds.; Springer: New York, NY, USA, 2005; pp. 645–657.
70. Argilaguet, J.; Pedragosa, M.; Esteve-Codina, A.; Riera, G.; Vidal, E.; Peligero-Cruz, C.; Casella, V.; Andreu, D.; Kaisho, T.; Bocharov, G.; et al. Systems analysis reveals complex biological processes during virus infection fate decisions. *Genome Res.* **2019**, *29*, 907–919. [CrossRef]
71. Omura, S.; Sato, F.; Park, A.-M.; Fujita, M.; Khadka, S.; Nakamura, Y.; Katsuki, A.; Nishio, K.; Gavins, F.N.E.; Tsunoda, I. Bioinformatics analysis of gut microbiota and CNS transcriptome in virus-induced acute myelitis and chronic inflammatory demyelination; potential association of distinct bacteria with CNS IgA upregulation. *Front. Immunol.* **2020**, *11*, 1138. [CrossRef] [PubMed]

72. Arad, I.D.; Alpan, G.; Sznajderman, S.D.; Eldor, A. The mean platelet volume (MPV) in the neonatal period. *Am. J. Perinatol.* **1986**, *3*, 1–3. [CrossRef] [PubMed]
73. Saxonhouse, M.A.; Garner, R.; Mammel, L.; Li, Q.; Muller, K.E.; Greywoode, J.; Miller, C.; Sola-Visner, M. Closure times measured by the platelet function analyzer PFA-100® are longer in neonatal blood compared to cord blood samples. *Neonatology* **2010**, *97*, 242–249. [CrossRef]
74. Sitaru, A.G.; Holzhauer, S.; Speer, C.P.; Singer, D.; Obergfell, A.; Walter, U.; Grossmann, R. Neonatal platelets from cord blood and peripheral blood. *Platelets* **2005**, *16*, 203–210. [CrossRef] [PubMed]
75. Rajasekhar, D.; Kestin, A.S.; Bednarek, F.J.; Ellis, P.A.; Barnard, M.R.; Michelson, A.D. Neonatal platelets are less reactive than adult platelets to physiological agonists in whole blood. *Thromb. Haemost.* **1994**, *72*, 957–963. [CrossRef]
76. Baker-Groberg, S.M.; Lattimore, S.; Recht, M.; McCarty, O.J.T.; Haley, K.M. Assessment of neonatal platelet adhesion, activation, and aggregation. *J. Thromb. Haemost.* **2016**, *14*, 815–827. [CrossRef]
77. Caparrós-Pérez, E.; Teruel-Montoya, R.; López-Andreo, M.J.; Llanos, M.C.; Rivera, J.; Palma-Barqueros, V.; Blanco, J.E.; Vicente, V.; Martinez, C.; Ferrer-Marin, F. Comprehensive comparison of neonate and adult human platelet transcriptomes. *PLoS ONE* **2017**, *12*, e0183042. [CrossRef]
78. Stolla, M.C.; Catherman, S.C.; Kingsley, P.D.; Rowe, R.G.; Koniski, A.D.; Fegan, K.; Vit, L.; McGrath, K.E.; Daley, G.Q.; Palis, J. Lin28b regulates age-dependent differences in murine platelet function. *Blood Adv.* **2019**, *3*, 72–82. [CrossRef] [PubMed]
79. Davenport, P.; Sola-Visner, M. Platelets in the neonate: Not just a small adult. *Res. Pract. Thromb. Haemost.* **2022**, *6*, e12719. [CrossRef] [PubMed]
80. Chapman, L.M.; Aggrey, A.A.; Field, D.J.; Srivastava, K.; Ture, S.; Yui, K.; Topham, D.J.; Baldwin, W.M., III; Morrell, C.N. Platelets present antigen in the context of MHC class I. *J. Immunol.* **2012**, *189*, 916–923. [CrossRef] [PubMed]
81. Guo, L.; Shen, S.; Rowley, J.W.; Tolley, N.D.; Jia, W.; Manne, B.K.; McComas, K.N.; Bolingbroke, B.; Kosaka, Y.; Krauel, K.; et al. Platelet MHC class I mediates $CD8^+$ T-cell suppression during sepsis. *Blood* **2021**, *138*, 401–416. [CrossRef] [PubMed]
82. Rivera-Quiñones, C.; McGavern, D.; Schmelzer, J.D.; Hunter, S.F.; Low, P.A.; Rodriguez, M. Absence of neurological deficits following extensive demyelination in a class I-deficient murine model of multiple sclerosis. *Nat. Med.* **1998**, *4*, 187–193. [CrossRef] [PubMed]
83. Tsunoda, I.; Fujinami, R.S. Neuropathogenesis of Theiler's murine encephalomyelitis virus infection, an animal model for multiple sclerosis. *J. Neuroimmune Pharmacol.* **2010**, *5*, 355–369. [CrossRef] [PubMed]
84. Li, Q.; Huang, D.; Nacion, K.; Bu, H.; Lin, F. Augmenting DAF levels in vivo ameliorates experimental autoimmune encephalomyelitis. *Mol. Immunol.* **2009**, *46*, 2885–2891. [CrossRef]
85. Ge, X.; Yu, Z.; Guo, X.; Li, L.; Ye, L.; Ye, M.; Yuan, J.; Zhu, C.; Hu, W.; Hou, Y. Complement and complement regulatory proteins are upregulated in lungs of COVID-19 patients. *Pathol. Res. Pract.* **2023**, *247*, 154519. [CrossRef]
86. Sadoul, K. New explanations for old observations: Marginal band coiling during platelet activation. *J. Thromb. Haemost.* **2015**, *13*, 333–346. [CrossRef] [PubMed]
87. Cuenca-Zamora, E.J.; Ferrer-Marín, F.; Rivera, J.; Teruel-Montoya, R. Tubulin in Platelets: When the Shape Matters. *Int. J. Mol. Sci.* **2019**, *20*, 3484. [CrossRef] [PubMed]
88. Diagouraga, B.; Grichine, A.; Fertin, A.; Wang, J.; Khochbin, S.; Sadoul, K. Motor-driven marginal band coiling promotes cell shape change during platelet activation. *J. Cell Biol.* **2014**, *204*, 177–185. [CrossRef] [PubMed]
89. Reddel, C.J.; Pennings, G.J.; Chen, V.M.; Gnanenthiran, S.R.; Kritharides, L. Colchicine as a modulator of platelet function: A systematic review. *Semin. Thromb. Hemost.* **2022**, *48*, 552–567. [CrossRef] [PubMed]
90. Kimura, M.Y.; Koyama-Nasu, R.; Yagi, R.; Nakayama, T. A new therapeutic target: The CD69-Myl9 system in immune responses. *Semin. Immunopathol.* **2019**, *41*, 349–358. [CrossRef]
91. Reusswig, F.; Polzin, A.; Klier, M.; Dille, M.A.; Ayhan, A.; Benkhoff, M.; Lersch, C.; Prinz, A.; Gorressen, S.; Fischer, J.W.; et al. Only acute but not chronic thrombocytopenia protects mice against left ventricular dysfunction after acute myocardial infarction. *Cells* **2022**, *11*, 3500. [CrossRef]
92. Zarbock, A.; Singbartl, K.; Ley, K. Complete reversal of acid-induced acute lung injury by blocking of platelet-neutrophil aggregation. *J. Clin. Investig.* **2006**, *116*, 3211–3219. [CrossRef]
93. D'Souza, C.S.; Li, Z.; Maxwell, D.L.; Trusler, O.; Murphy, M.; Crewther, S.; Peter, K.; Orian, J.M. Platelets drive inflammation and target gray matter and the retina in autoimmune-mediated encephalomyelitis. *J. Neuropathol. Exp. Neurol.* **2018**, *77*, 567–576. [CrossRef]
94. Martinez, N.E.; Karlsson, F.; Sato, F.; Kawai, E.; Omura, S.; Minagar, A.; Grisham, M.B.; Tsunoda, I. Protective and detrimental roles for regulatory T cells in a viral model for multiple sclerosis. *Brain Pathol.* **2014**, *24*, 436–451. [CrossRef]
95. Mosmann, T.R.; Coffman, R.L. TH1 and TH2 cells: Different patterns of lymphokine secretion lead to different functional properties. *Annu. Rev. Immunol.* **1989**, *7*, 145–173. [CrossRef] [PubMed]
96. Mosmann, T.R.; Coffman, R.L. Heterogeneity of cytokine secretion patterns and functions of helper T cells. *Adv. Immunol.* **1989**, *46*, 111–147. [CrossRef] [PubMed]
97. Rodriguez, M.; Zoecklein, L.J.; Howe, C.L.; Pavelko, K.D.; Gamez, J.D.; Nakane, S.; Papke, L.M. Gamma interferon is critical for neuronal viral clearance and protection in a susceptible mouse strain following early intracranial Theiler's murine encephalomyelitis virus infection. *J. Virol.* **2003**, *77*, 12252–12265. [CrossRef] [PubMed]

98. Binder, G.K.; Griffin, D.E. Interferon-γ-mediated site-specific clearance of alphavirus from CNS neurons. *Science* **2001**, *293*, 303–306. [CrossRef] [PubMed]
99. Patterson, C.E.; Lawrence, D.M.P.; Echols, L.A.; Rall, G.F. Immune-mediated protection from measles virus-induced central nervous system disease is noncytolytic and gamma interferon dependent. *J. Virol.* **2002**, *76*, 4497–4506. [CrossRef] [PubMed]
100. Fairweather, D.; Frisancho-Kiss, S.; Yusung, S.A.; Barrett, M.A.; Davis, S.E.; Gatewood, S.J.; Njoku, D.B.; Rose, N.R. Interferon-γ protects against chronic viral myocarditis by reducing mast cell degranulation, fibrosis, and the profibrotic cytokines transforming growth factor-β_1, interleukin-1β, and interleukin-4 in the heart. *Am. J. Pathol.* **2004**, *165*, 1883–1894. [CrossRef] [PubMed]
101. Yamamoto, N.; Shibamori, M.; Ogura, M.; Seko, Y.; Kikuchi, M. Effects of intranasal administration of recombinant murine interferon-γ on murine acute myocarditis caused by encephalomyocarditis virus. *Circulation* **1998**, *97*, 1017–1023. [CrossRef] [PubMed]
102. Park, A.-M.; Tsunoda, I. Forensic luminol reaction for detecting fecal occult blood in experimental mice. *Biotechniques* **2018**, *65*, 227–230. [CrossRef]
103. Harrington, R.A.; Stone, G.W.; McNulty, S.; White, H.D.; Lincoff, A.M.; Gibson, C.M.; Pollack, C.V., Jr.; Montalescot, G.; Mahaffey, K.W.; Kleiman, N.S.; et al. Platelet inhibition with cangrelor in patients undergoing PCI. *N. Engl. J. Med.* **2009**, *361*, 2318–2329. [CrossRef]
104. Bhatt, D.L.; Stone, G.W.; Mahaffey, K.W.; Gibson, C.M.; Steg, P.G.; Hamm, C.W.; Price, M.J.; Leonardi, S.; Gallup, D.; Bramucci, E.; et al. Effect of platelet inhibition with cangrelor during PCI on ischemic events. *N. Engl. J. Med.* **2013**, *368*, 1303–1313. [CrossRef]
105. Becker, R.C.; Bassand, J.P.; Budaj, A.; Wojdyla, D.M.; James, S.K.; Cornel, J.H.; French, J.; Held, C.; Horrow, J.; Husted, S.; et al. Bleeding complications with the $P2Y_{12}$ receptor antagonists clopidogrel and ticagrelor in the PLATelet inhibition and patient Outcomes (PLATO) trial. *Eur. Heart J.* **2011**, *32*, 2933–2944. [CrossRef]
106. Baurand, A.; Raboisson, P.; Freund, M.; Léon, C.; Cazenave, J.-P.; Bourguignon, J.-J.; Gachet, C. Inhibition of platelet function by administration of MRS2179, a $P2Y_1$ receptor antagonist. *Eur. J. Pharmacol.* **2001**, *412*, 213–221. [CrossRef]
107. Dunne, H.; Cowman, J.; Kenny, D. MRS2179: A novel inhibitor of platelet function. *BMC Proc.* **2013**, *9*, A2. [CrossRef]
108. The Epic Investigators. Use of a monoclonal antibody directed against the platelet glycoprotein IIb/IIIa receptor in high-risk coronary angioplasty. *N. Engl. J. Med.* **1994**, *330*, 956–961. [CrossRef]
109. Moeckel, D.; Jeong, S.S.; Sun, X.; Broekman, M.J.; Nguyen, A.; Drosopoulos, J.H.F.; Marcus, A.J.; Robson, S.C.; Chen, R.; Abendschein, D. Optimizing human apyrase to treat arterial thrombosis and limit reperfusion injury without increasing bleeding risk. *Sci. Transl. Med.* **2014**, *6*, 248ra105. [CrossRef] [PubMed]
110. Daniels, J.B.; Pappenheimer, A.M.; Richardson, S. Observations on encephalomyelitis of mice (DA strain). *J. Exp. Med.* **1952**, *96*, 517–530. [CrossRef] [PubMed]
111. National Research Council (US) Committee for the Update of the Guide for the Care and Use of Laboratory Animals. *Guide for the Care and Use of Laboratory Animals*, 8th ed.; National Academies Press: Washington, DC, USA, 2011.
112. Senchenkova, E.Y.; Ansari, J.; Becker, F.; Vital, S.A.; Al-Yafeai, Z.; Sparkenbaugh, E.M.; Pawlinski, R.; Stokes, K.Y.; Carroll, J.L.; Dragoi, A.-M.; et al. Novel role for the AnxA1-Fpr2/ALX signaling axis as a key regulator of platelet function to promote resolution of inflammation. *Circulation* **2019**, *140*, 319–335. [CrossRef] [PubMed]
113. R Core Team. *R: A Language and Environment for Statistical Computing*; R Foundation for Statistical Computing: Vienna, Austria, 2023.
114. Sun, J.; Nishiyama, T.; Shimizu, K.; Kadota, K. TCC: An R package for comparing tag count data with robust normalization strategies. *BMC Bioinform.* **2013**, *14*, 219. [CrossRef] [PubMed]
115. Ringnér, M. What is principal component analysis? *Nat. Biotechnol.* **2008**, *26*, 303–304. [CrossRef] [PubMed]
116. Loke, P.; Favre, D.; Hunt, P.W.; Leung, J.M.; Kanwar, B.; Martin, J.N.; Deeks, S.G.; McCune, J.M. Correlating cellular and molecular signatures of mucosal immunity that distinguish HIV controllers from noncontrollers. *Blood* **2010**, *115*, e20–e32. [CrossRef]
117. Davies, D.L.; Bouldin, D.W. A cluster separation measure. *IEEE Trans. Pattern Anal. Mach. Intell.* **1979**, *1*, 224–227. [CrossRef] [PubMed]
118. Sood, R.; Sholl, L.; Isermann, B.; Zogg, M.; Coughlin, S.R.; Weiler, H. Maternal Par4 and platelets contribute to defective placenta formation in mouse embryos lacking thrombomodulin. *Blood* **2008**, *112*, 585–591. [CrossRef] [PubMed]
119. Sato, F.; Nakamura, Y.; Katsuki, A.; Khadka, S.; Ahmad, I.; Omura, S.; Martinez, N.E.; Tsunoda, I. Curdlan, a microbial β-glucan, has contrasting effects on autoimmune and viral models of multiple sclerosis. *Front. Cell Infect. Microbiol.* **2022**, *12*, 805302. [CrossRef] [PubMed]
120. Sato, F.; Kawai, E.; Martinez, N.E.; Omura, S.; Park, A.-M.; Takahashi, S.; Yoh, K.; Tsunoda, I. T-bet, but not Gata3, overexpression is detrimental in a neurotropic viral infection. *Sci. Rep.* **2017**, *7*, 10496. [CrossRef]
121. Nitayaphan, S.; Toth, M.M.; Roos, R.P. Neutralizing monoclonal antibodies to Theiler's murine encephalomyelitis viruses. *J. Virol.* **1985**, *53*, 651–657. [CrossRef]